MODELING, ANALYSIS AND EXPERIMENTAL VERIFICATION OF VARIABLE-SPEED CONSTANT-FREQUENCY POWER CONVERSION SCHEME WITH A PERMANENT MAGNET SYNCHRONOUS GENERATOR

by

Geun-hie Rim

Thesis submitted to the Faculty of the

Virginia Polytechnic Institute and State University

in partial fulfillment of the requirements for the degree of

Master of Science

in

Electrical Engineering

APPROVED:

Krishnan Ramu

Dr. Krishnan Ramu :Committee Chair

Saifur Rahman

Dr. Saifur Rahman

Dr. Kwa-Sur Tam

February,1988

Blacksburg, Virginia

MODELING, ANALYSIS AND EXPERIMENTAL VERIFICATION OF VARIABLE-SPEED CONSTANT-FREQUENCY POWER CONVERSION SCHEME WITH A PERMANENT MAGNET SYNCHRONOUS GENERATOR

by

Geun-hie Rim

Dr. Krishnan Ramu :Committee Chair

Electrical Engineering

(ABSTRACT)

A variable-speed constant frequency (VSCF) power conversion scheme with a permanent magnet synchronous generator (PMSG) is studied in this dissertation. The scheme consists of a PMSG, diode-rectifier bridge, dc link filter, controlled converter for conversion to the constant frequency ac utility and transformer. The various subsystems listed above are modeled for steady state analysis and the simulation results are experimentally verified. All the relevant performance equations are derived for both the three phase half-wave (THWI) and full-wave (TFWI) controlled converter options and the harmonics are computed.

Acknowledgements

To many I owe my gratitude for the support I received during the course of this thesis research. In particular, I am fortunate to receive the guidance of Dr. Krishnan Ramu. I am also indebted to Korea Electrotechnology Research Institute for their support. This work was made possible by the steadfast support and sacrifice of my family. To them I owe my gratitude.

Table of Contents

Chapter 1. Introduction

1.1 Introduction

This chapter outlines the literature survey, problem formulation, scope and organization of the thesis.

1.2 Literature survey

Energy sources operating over a wide speed range are required to produce constant frequency for transmission and use. Synchronous machines used for power generation with variable-speed prime movers produce variable voltage variable frequency sources. The output can be processed through power converters such as cycloconverters or rectifier - dc link - inverter to provide fixed voltage and constant frequency power supply [1,2]. Induction machines have been investigated for this purpose in [3,4]. Even though various advantages have been identified for using induction machines, they have the following disadvantages:

i. Requirement of a constant frequency power supply to provide magnetization. This may not be available in an island or if the utility connection has a malfunction.

ii. Large KVAR required from the utility (external source).

iii. Low efficiency and low power factor.

iv. Redesign of rotors to yield large induced emf.

v. Need for slip-rings and hence the enhanced cost of the machines.

Most of these disadvantages can be overcome with wound rotor synchronous machines excepting (i) and (v). They too are offset using permanent magnet synchronous generators(PMSG). They have the following unique features:

i. Permanent magnet excitation.

ii. High power factor.

iii. High efficiency.

iv. No slip-rings on the rotor.

v. Compact construction and high power density.

All these features are attractive both for small and large installations. The fact that PMSG can be designed to provide sinusoidal or trapezoidal emfs and lend themselves to design flexibility at the power conversion stage. With high-temperature superconducting materials becoming a reality in the near future, the study of variable speed constant frequency (VSCF) power conversion with PM/superconducting synchronous generators is important. Note that the study of PMSG is directly applicable to the superconducting synchronous generator scheme with hardly any change at all.

1.3 Scope of the thesis

This thesis research is concerned with the study of VSCF power conversion with synchronous generator. The power conversion link involves an ac-rectifer, dc-link, controlled converter and constant frequency source. Steady state modeling of the entire scheme with half and full-wave controlled converter stages, simulation and analysis have been completed and experimental correlation is provided from a laboratory prototype constructed exclusively for this thesis. The performance characteristics of interest include real power, reactive power, power factor, efficiency, control angle of the converter, dc-link characteristics and harmonics on the machine and utility sides as a function of the speed of the PMSG.

1.4 Organization of the thesis

This thesis is organized as follows. The steady state modeling and analysis of the VSCF power conversion with PMSG are presented in chapter 2 along with system losses and overall efficiency calculations. The harmonics of the voltages and currents are analyzed in chapter 3 for both the half and full-wave converter cases. Chapter 4 contains the correlation of the experimental results with the predicted values. Conclusions are given in chapter 5.

2. Modeling and analysis of VSCF power conversion scheme with PMSG

2.1 Introduction

The VSCF power conversion scheme with PMSG is described in this chapter. The various subsystems such as PMSG and converters are modeled for steady state operation. Performance characteristics are derived relating the speed of the PMSG, torque and triggering angle of the controlled converters.

2.2 VSCF power conversion with PMSG

The scheme considered for study in this dissertation is shown in figure 2.1. The PMSG has sinusoidal induced emfs. The output of the PMSG is rectified through a three-phase full-wave diode rectifier and is connected to a filter choke. The dc link output is fed as input into a phase controlled converter supplied from a three-phase

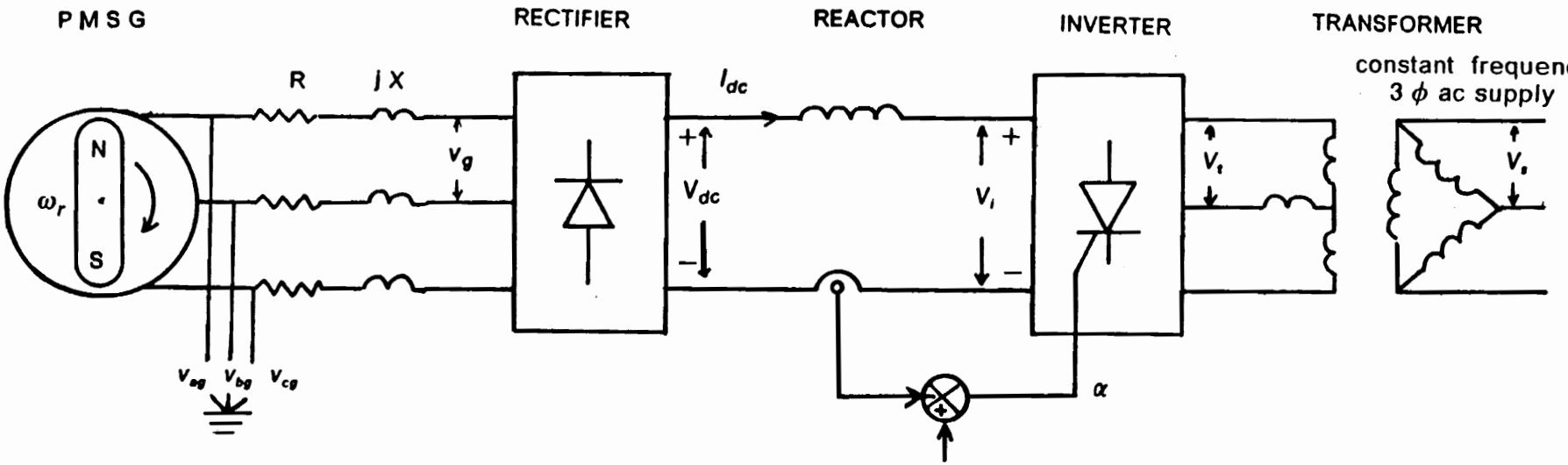

Figure 2.1 The overall energy conversion scheme

constant-frequency supply through a transformer. The transformer is optional but included at this stage so as to cover a comprehensive study. Depending on the magnitude of induced emf in the PMSG and available fixed frequency line supply, the transformer need is determined.

The process of power conversion can be summed as follows: the output of the PMSG is rectified and regenerated through the controlled converter to the fixed frequency ac supply.

2.3 Permanent magnet synchronous generator

The use of permanent magnet material in the rotor provides the excitation for a synchronous machine eliminating the necessity of a source for excitation and slip rings on the rotor.

A PM rotor can be adequately represented by a constant field current consisting of a source of a constant distributed mmf in series with the nonlinear reluctance of the rotor magnet material. Because of the nonlinear reluctance, the magnetizing reactance is generally a nonlinear function of the magnetizing current or the induced voltage. However, if the machine is operated over a reasonable range of voltage, a suitable average value of magnetizing reactance can be used for this operating range. When a PM machine is modeled into an electrcal equivalent circuit, a constant current source and the reactance, connected in parallel, can represent the constant magnetomotive force and the reluctance, respectively, by the duality concept. Compared with that of the normal machine, the excitation of the PM machine is not adjustible.

A salient-pole machine is a typical synchronous machine, and it has the combined features of the reluctance machine and the wound rotor synchronous machine. Its equivalent circuit, shown in figure 2.2, includes a current source that represents the magnetomotive force produced by the rotor field. Applying Thevenin's theorem, an alternative equivalent circuit can be obtained, as shown in figure 2.3:

$$
\begin{aligned}
Z_{eq} &= j x_d \parallel \left[- \frac{x_d x_q}{x_d - x_q} \cot \beta + j \frac{x_d x_q}{x_d - x_q} \right] \\
&= \frac{x_d x_q + j x_d x_q \cot \beta}{x_q \cot \beta - j x_d} \\
&= \frac{x_d x_q^2 \cot \beta - x_d^2 x_q \cot \beta}{x_q^2 \cot^2 \beta + x_d^2} + j \frac{x_d x_q^2 \cot^2 \beta + x_d^2 x_q}{x_q^2 \cot^2 \beta + x_d^2} \\
&= R_{eq} + j X
\end{aligned}
\tag{2.1}
$$

where

$$
R_{eq} = \frac{x_d x_q^2 \cot \beta - x_d^2 x_q \cot \beta}{x_q^2 \cot^2 \beta + x_d^2} \tag{2.2}
$$

$$
X = \frac{x_d x_q^2 \cot^2 \beta + x_d^2 x_q}{x_q^2 \cot^2 \beta + x_d^2} \tag{2.3}
$$

$$
X_d = W_r L_d \tag{2.4}
$$

$$
X_q = W_r L_q \tag{2.5}
$$

and L_d, L_q, β are quadrature d,q axes inductances, the rotor angle, respectively.

Therefore the total impedance observed on the stator terminal is

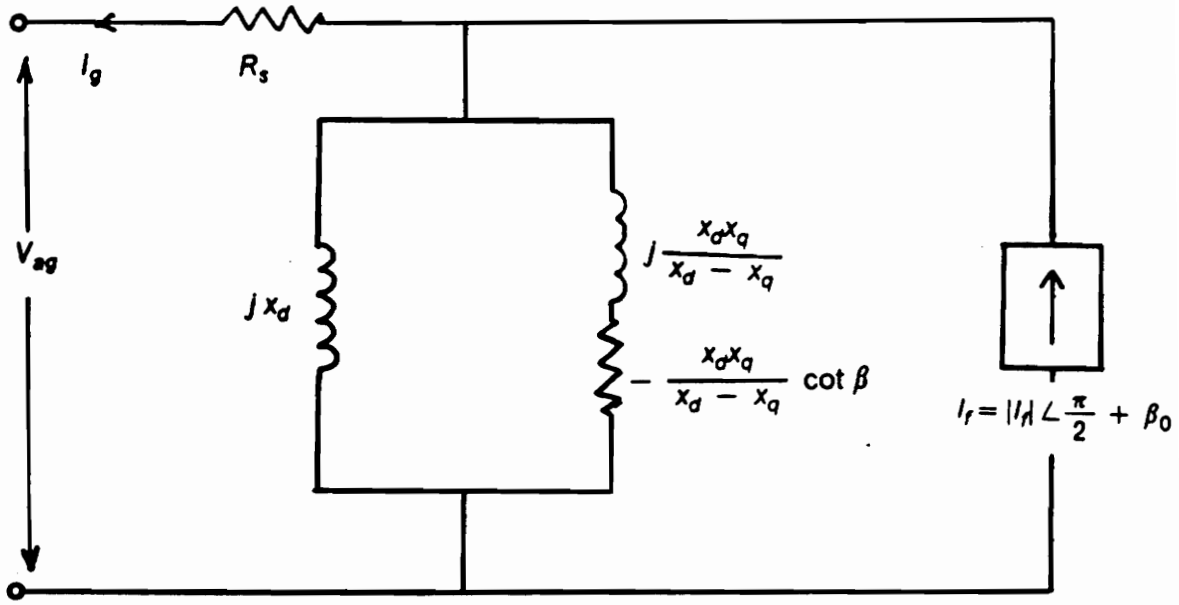

Figure 2.2 Equivalent circuit for salient-pole synchronous machine

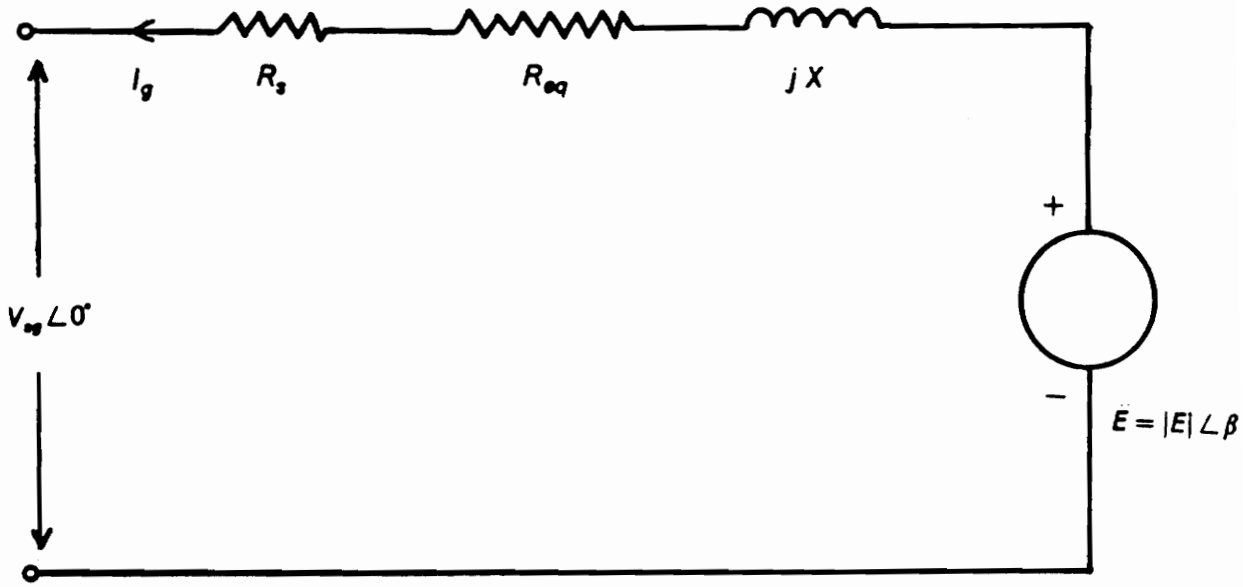

Figure 2.3 Thevenin equivalent of figure 2.2

$$Z = R_s + R_{eq} + jX$$
$$= R + jX \tag{2.6}$$

where

$$R = R_s + R_{eq} \tag{2.7}$$

In the alternative equivalent circuit, the relation between the equivalent emf and the current source is

$$E = Z\ I_f \tag{2.8}$$

where I_f is a field current. And the induced emf E is

$$|E| = \lambda_{af}\,\omega_r \tag{2.9}$$

where λ_{af} [*V sec./rad.*] is the mutual flux linkage between rotor and stator due to the magnet and ω_r [*rad./sec.*] is the rotor speed. Therefore the phase voltage at the stator terminal is

$$V_{ag} = E - I_g Z \tag{2.10}$$

where I_g is the PMSG phase current. The power output per phase of the machine in the steady state is

$$P_s = Re[\bar{I}_g V_{ag}] \tag{2.11}$$

But, this output with the equivalent resistance loss being subtracted should be the same as the power which flows through the rectifier.

$$
\begin{aligned}
P_s &= 3\, I_{g1}\, |V_{ag}|\, \cos\, (\angle I_{g1} - \angle V_{ag}) \\
&= \frac{3\sqrt{3}}{\sqrt{2}\,\pi} I_{dc} |V_{ag}| \cos\phi \\
&= 3\times 0.779\; I_{dc}\, |V_{ag}|\, \cos\phi
\end{aligned}
\tag{2.12}
$$

where I_{g1} is the fundamental of the generator phase current during rectification, and ϕ is the phase difference between the fundamental current and the phase voltage.

Neglecting the stator loss, the air gap power is equal to P_s, which means that the torque for steady state operation is given by

$$
T = P_s / w_r \tag{2.13}
$$

If the torque is constant, the generated power is proportional to the rotor speed.

2.4 Rectifier

The three phase power generated by PMSG is rectified through a three-phase, full-wave diode bridge rectifier. The advantage of using the diode bridge rectifier is that it has a line power factor of nearly unity. Its operation in connection with the PMSG is shown in figure 2.4.

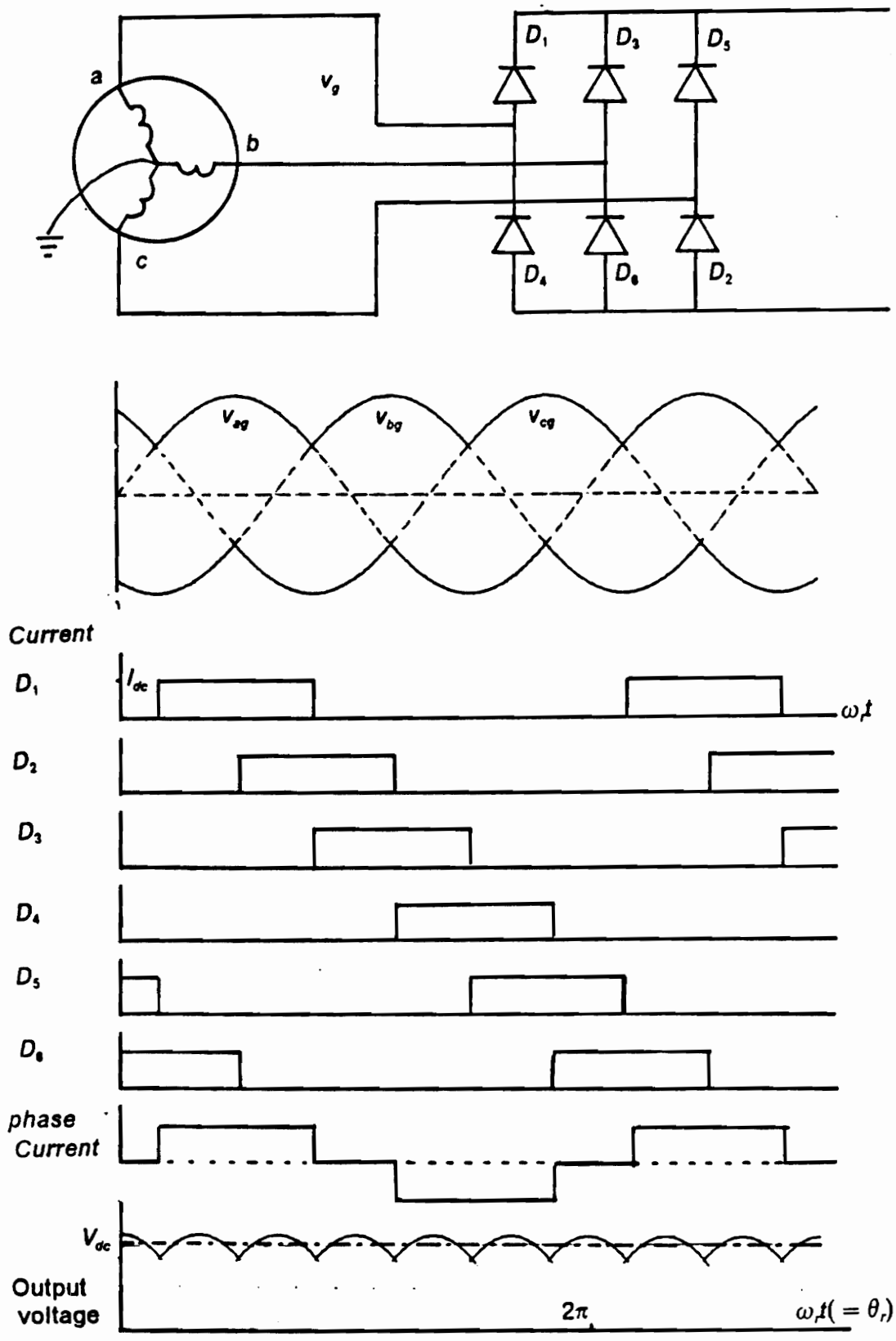

Figure 2.4 The three phase full-wave bridge rectifier

2.4.1 Overlap angle

The dc voltage at the rectifier dc terminal is given by

$$
\begin{aligned}
V_{dc} &= \frac{1}{\frac{\pi}{3}} \int_{\frac{\pi}{3}}^{\frac{2\pi}{3}} v_g d\omega_r t \\
&= \frac{3}{\pi} \int_{\frac{\pi}{3}}^{\frac{2\pi}{3}} V_{gm} \sin \omega t d\theta r \\
&= \frac{3}{\pi} V_{gm} \\
&= \frac{3\sqrt{2}}{\pi} \left(\frac{V_{gm}}{\sqrt{2}}\right)
\end{aligned}
\tag{2.14}
$$

where

$$v_g = V_{gm} \sin \omega_r t \tag{2.15}$$

$$\theta_r = \omega_r t \tag{2.16}$$

However, the phase inductances in the PMSG prevent the instantaneous transfer of diode currents. Consequently, there is a commutation period or an overlap angle μ during which the two phases of the PMSG stator are short-circuited through diodes. Therefore, during the overlap, the load is reduced to zero and only the PMSG equivalent inductance determines the rate of rise of current in the diodes.

For the PMSG equivalent phase inductance, the voltage lost during overlap is

$$
\begin{aligned}
V_{OL} &= \frac{3}{\pi}\int_{\frac{\pi}{6}}^{\frac{\pi}{6}+\mu}\frac{1}{2}(v_{ag}-v_{cg})d\theta_r \\
&= \frac{3}{\pi}\int_{\frac{\pi}{6}}^{\frac{\pi}{6}+\mu}\frac{1}{2}V_m[\sin\theta_r-\sin(\theta_r+\frac{2\pi}{3})]d\theta_r \\
&= \frac{3\sqrt{3}\,V_m}{2\pi}(1-\cos\mu)
\end{aligned}
\tag{2.17}
$$

But the magnitude of the overlap voltages is

$$V_{OL} = X\,I_{dc} \tag{2.18}$$

Hence, equating equations (2.17) and (2.18), the overlap angle μ is given by

$$
\begin{aligned}
\mu &= \cos^{-1}[1-\frac{2\pi X I_{dc}}{3\sqrt{3}\,V_m}] \\
&= \cos^{-1}[1-\frac{2\pi X I_{dc}}{3V_{gm}}]
\end{aligned}
\tag{2.19}
$$

The presence of overlap tends to increase the phase lag of the fundamental current, which results in the generator power factor being less than unity.

2.4.2 Diode current due to overlap angle

During commutating period μ, one of the two conducting diodes' currents i_1 shown in figure 2.5 gradually reduces to zero, while the other current i_2 gradually increases to I_{dc}. If the inductance in the dc link circuit is so large that the load current I_{dc} remains constant:

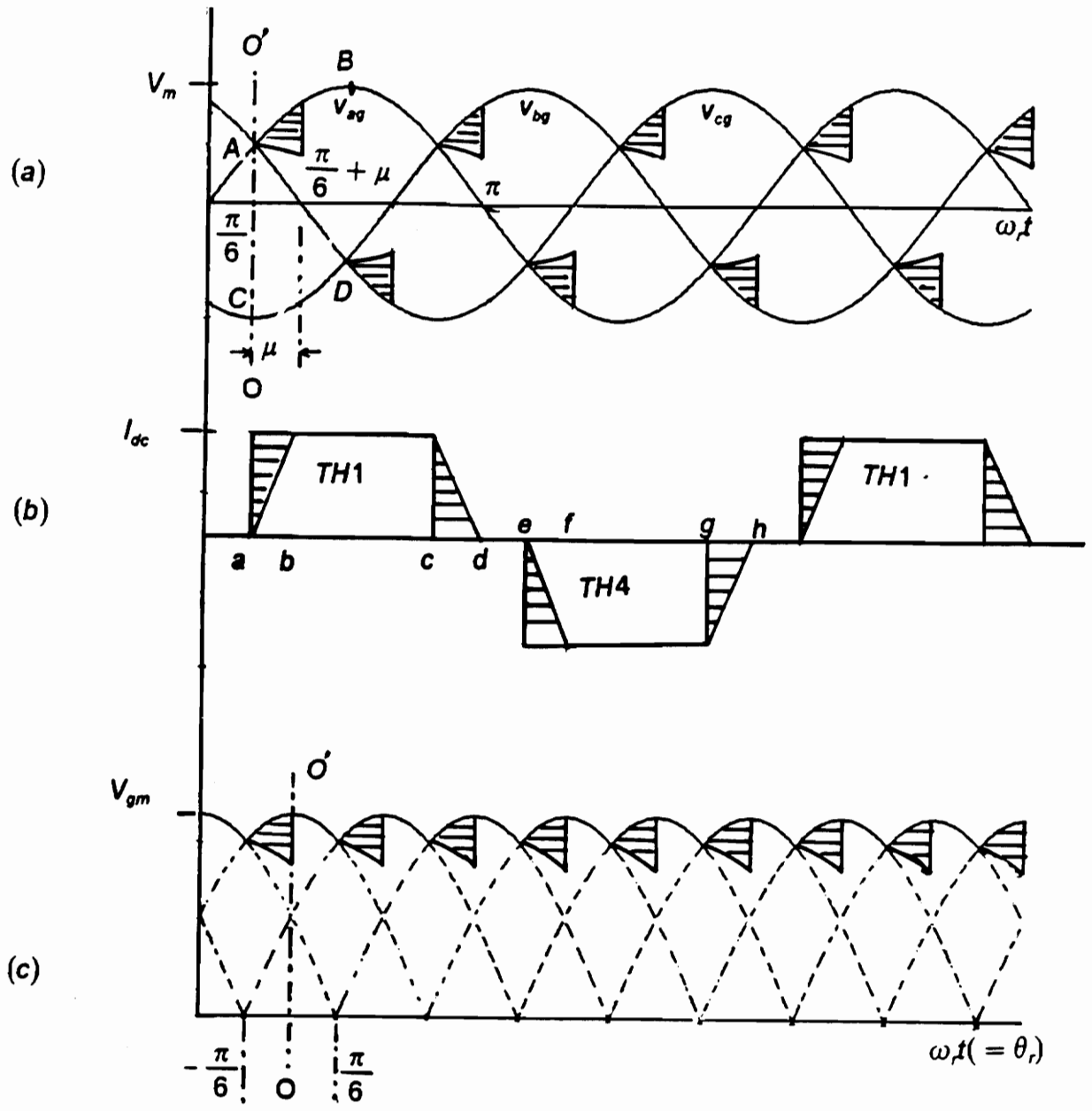

Figure 2.5 Waveforms of the generator:
(a) Phase voltage of the generator;
(b) Line current of the rectifier ac side;
(c) Output Voltage of the Rectifier;

$$I_{dc} = i_1 + i_2 \tag{2.20}$$

During the overlap, the dc link voltage is the average of the corresponding instantaneous PMSG stator phase voltage v_{ag}, $v_{bg}$and v_{cg}, and then, similarly successive diodes take over. Neglecting the resistance of the PMSG equivalent winding resistance,

$$v_{cg} - L\frac{di_1}{dt} - v_r = v_{ag} - L\frac{di_2}{dt} - v_r \tag{2.21}$$

where

$$L = \frac{X}{\omega_r} \tag{2.22}$$

Hence,

$$v_{cg} - v_{ag} = L(\frac{di_1}{dt} - \frac{di_2}{dt}) \tag{2.23}$$

If the stator terminal voltages $v_{ag}$and v_{cg} are referred to the origin oo′ , they are expressed as follows:

$$v_{cg} = V_m \cos(\omega_r t + \frac{\pi}{3}) \tag{2.24}$$

$$v_{ag} = V_m \cos(\omega_r t - \frac{\pi}{3}) \tag{2.25}$$

Substituting equations (2.24) and (2.25) into equation (2.23) yields:

$$L\left(\frac{di_1}{dt} - \frac{di_2}{dt}\right) = -\sqrt{3}\, V_m \sin \omega_r t$$
$$= - V_{gm} \sin \omega_r t \tag{2.26}$$

But, from equation (2.20), i_1 and i_2 have the relation as follows:

$$\frac{di_1}{dt} + \frac{di_2}{dt} = 0. \tag{2.27}$$

Combining equations (2.25) and (2.26) results in

$$\frac{di_2}{dt} = \frac{V_{gm}}{2L} \sin \omega_r t \tag{2.28}$$

Hence,

$$i_2 = \int_0^{i_2} di_2$$
$$= \frac{V_{gm}}{2L} \int_0^t \sin \omega_r t dt \tag{2.29}$$
$$= \frac{V_{gm}}{2\omega_r L}(1 - \cos \omega_r t)$$

Introducing the following boundary condition

$$i_2(t) = I_{dc} \tag{2.30}$$

$$\text{at} \quad \omega_r t = \mu \tag{2.31}$$

$$I_{dc} = \frac{V_{gm}}{2\omega_r L}(1 - \cos \mu) \tag{2.32}$$

From equations (2.20) and (2.29),

$$
\begin{aligned}
i_1 &= I_{dc} - i_2 \\
&= I_{dc} - \frac{V_{gm}}{2\omega_r L}(1 - \cos\omega_r t) \\
&= I_{dc} - \frac{I_{dc}}{1 - \cos\mu}(1 - \cos\omega_r t) \\
&= I_{dc}\left(1 - \frac{1 - \cos\omega_r t}{1 - \cos\mu}\right)
\end{aligned}
\tag{2.33}
$$

2.4.3 DC link voltage with overlap angle

Considering the overlap effect, the dc link voltage can be obtained. The hatched area in figure 2.5 is the voltage reduced due to the overlap, which results in the reduction of the average dc voltage. The area ABCD , divided by $\frac{\pi}{3}$, would be the average dc voltage, neglecting thyristor voltage drop.

$$
\begin{aligned}
V_{dc} &= \frac{3}{\pi}\int_{\frac{\pi}{6}}^{\frac{\pi}{2}} v_{ag} - v_{bg}\, d\theta_r \\
&= \frac{3\sqrt{3}\,V_m}{\pi} \\
&= \frac{3\sqrt{2}}{\pi}\left(\frac{V_{gm}}{\sqrt{2}}\right)
\end{aligned}
\tag{2.34}
$$

Compared to the overlap voltage drop, other voltage drops are negligible. The net average dc link voltage can be obtained, therefore, by subtracting the overlap voltage drop (the hatched area) from the area ABCD.

From equation (2.17), the hatched area V_{oL} is

$$V_{OL} = \frac{3V_{gm}}{2\pi}\ (1\ -\ \cos\mu) \tag{2.35}$$

The net average dc voltage is, therefore,

$$\begin{aligned} V_{dc} &= \frac{3V_{gm}}{2\pi}(1\ +\cos\mu) \\ &= \frac{3V_{gm}}{\pi}\ -\ XI_{dc} \end{aligned} \tag{2.36}$$

2.5 DC link reactor

The purpose of the dc link filter in this scheme is to provide a sustantially smooth dc current. Considering only the dominant 6^{th} harmonic, for a full wave rectifier, the voltage and current wave forms are as shown in figure 2.6. If the overlap angle is not considered, the reactance L_{dc} can be calculated as in the following :

$$\begin{aligned} L_{dc}\frac{\Delta I_{dc}}{\Delta t} &= \int_{t_1}^{t_2}(V_{gm}\sin\omega_r t\ -\ V_{dc})dt \\ &= \int_{t_1}^{t_2}(V_{gm}\sin\omega_r t\ -\ \frac{3}{\pi}V_{gm})dt \\ &= V_{gm}[\ -\ \frac{1}{\omega_r}(\cos\omega_r t_2\ -\ \cos\omega_r t_1)\ -\ \frac{3}{\pi}(t_2\ -\ t_1)] \\ &= \frac{V_{gm}}{\omega_r}[\ \cos(\sin^{-1}\frac{3}{\pi})\ -\ \cos(\pi\ -\ \sin^{-1}\frac{3}{\pi})\ -\ \frac{3}{\pi}(\pi\ -\ 2\sin^{-1}\frac{3}{\pi})] \end{aligned} \tag{2.37}$$

which amounts to

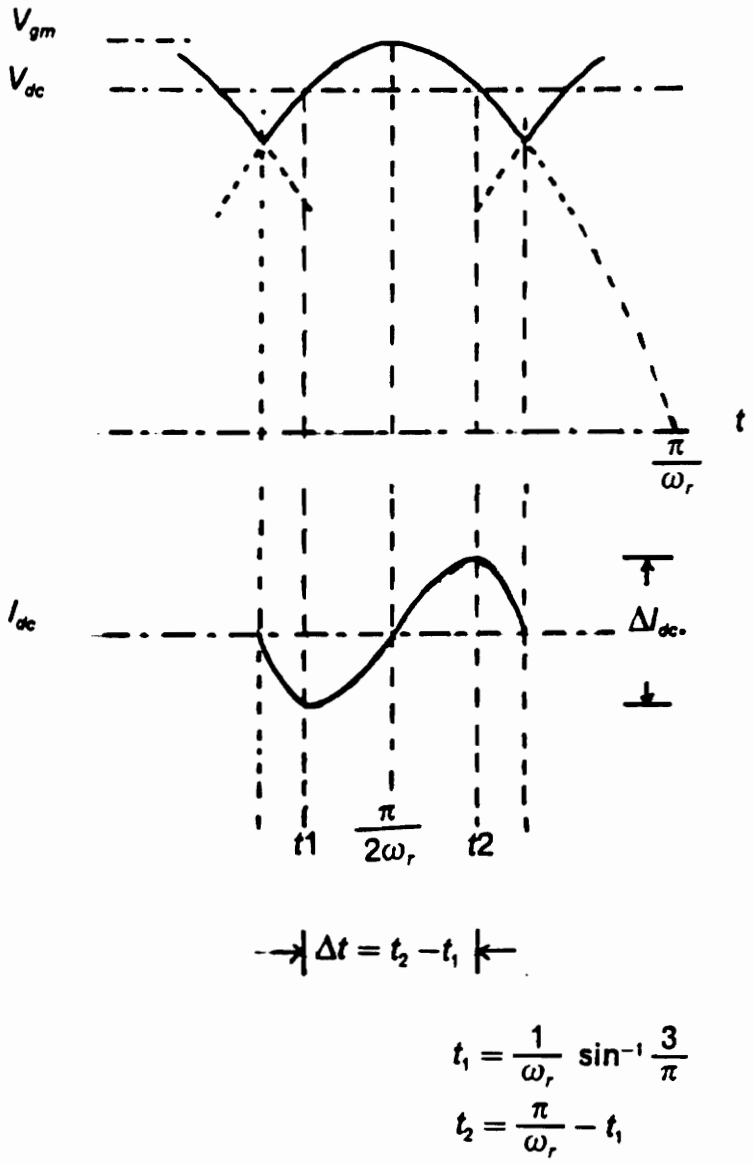

Figure 2.6 Output waveforms in a rectifier with Critical Inductance

$$L_{dc} = \frac{\pi}{3}\frac{V_{dc}}{\omega_r^2 \Delta I_{dc}}(\pi - 2\sin^{-1}\frac{3}{\pi}) \times$$
$$[\cos(\sin^{-1}\frac{3}{\pi}) - \cos(\pi - \sin^{-1}\frac{3}{\pi}) - \frac{3}{\pi}(\pi - 2\sin^{-1}\frac{3}{\pi})] \quad (2.38)$$

If the overlap angle is considered , L_{dc} can be obtained by replacing V_{dc} as given in equation (2.36).

$$L_{dc} = \frac{\pi}{3}(\frac{3V_{gm}}{\pi} - X I_{dc})\ (\pi - 2\sin^{-1}\frac{3}{\pi}) \times$$
$$[\cos(\sin^{-1}\frac{3}{\pi}) - \cos(\pi - \sin^{-1}\frac{3}{\pi}) - \frac{3}{\pi}(\pi - 2\sin^{-1}\frac{3}{\pi})] \quad (2.39)$$

2.6 Inverter

Inversion mode pertaining to the dc and ac conversion is investigated in this section. The substantially smooth dc current is input into the constant frequency ac bus through a phase controlled inverter. Two inverter schemes are investigated; one is a three-phase half-wave inverter and the other is a three-phase full-wave inverter.

The triggering angle of an inverter is from 90° to 180° . However, the actual control is limited from 90° to 155° because of the minimum time required for turning off the SCRs. Both the inverter configurations are investigated with overlap and without overlap of the current.

The delay angle α is introduced by phase control resulting in the retardation of the current pulses. The power factor is, therefore, the cosine of the delay angle. The

harmonics in current, however, are not changed due to the phase control because there is no change in the current waveforms.

2.6.1 Three phase half-wave inverter

The three-phase half-wave thyristor controlled inverter is shown in figure 2.7. The inversion mode neglecting the overlap due to the transformer equivalent reactance is shown in figures 2.8 and 2.9. The transfer characteristics can be derived as in the following:

$$\begin{aligned} V_i &= = \frac{1}{\frac{2\pi}{3}} \int_{\frac{\pi}{6}+\alpha}^{\frac{5\pi}{6}+\alpha} v_{at}\, d\omega_s t \\ &= \frac{3}{2\pi} \int_{\frac{\pi}{6}+\alpha}^{\frac{5\pi}{6}+\alpha} \frac{V_{tm}}{\sqrt{3}} \sin \omega_s t d\omega_s t \\ &= \frac{3\sqrt{2}\, V_t}{2\pi} \cos \alpha \; ; \quad 90° \leq \alpha \leq 155° \end{aligned} \tag{2.40}$$

The transfer characteristic of the voltage is shown in figure 2.10. The thyristor current neglecting the overlap angle may be expressed by a Fourier series:

$$\begin{aligned} i_{dc}(t) = \frac{1}{3} I_{dc} \; + \; \frac{I_{dc}}{\pi} \frac{1}{n} \sum_{n=1}^{\infty} [\{ \sin \; n(\frac{5\pi}{6} + \alpha) - \; \sin \; n(\frac{\pi}{6} + \alpha)\} \; \cos \; n\omega_s t \; + \\ \{ \cos \; n(\frac{\pi}{6} + \alpha) - \cos \; n(\frac{5\pi}{6} + \alpha)\} \sin \; n\omega_s t] \end{aligned} \tag{2.41}$$

The fundamental component of the current is

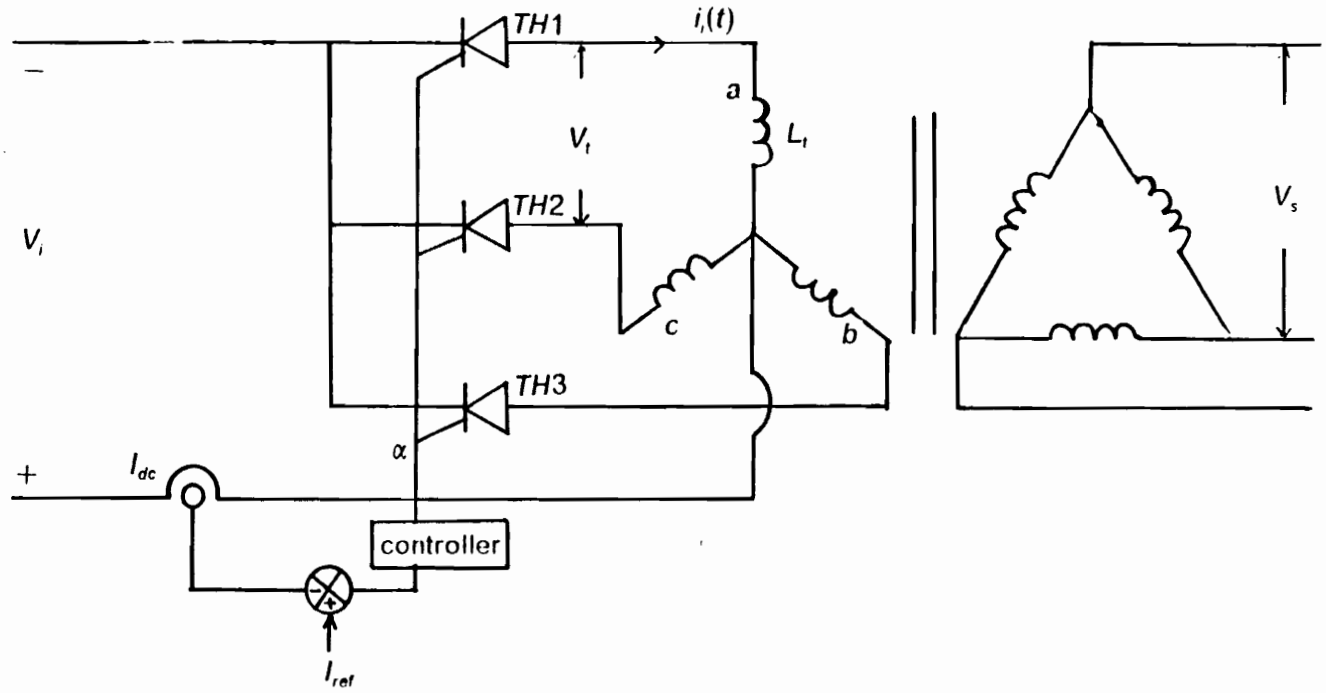

Figure 2.7 Three phase half-wave inverter

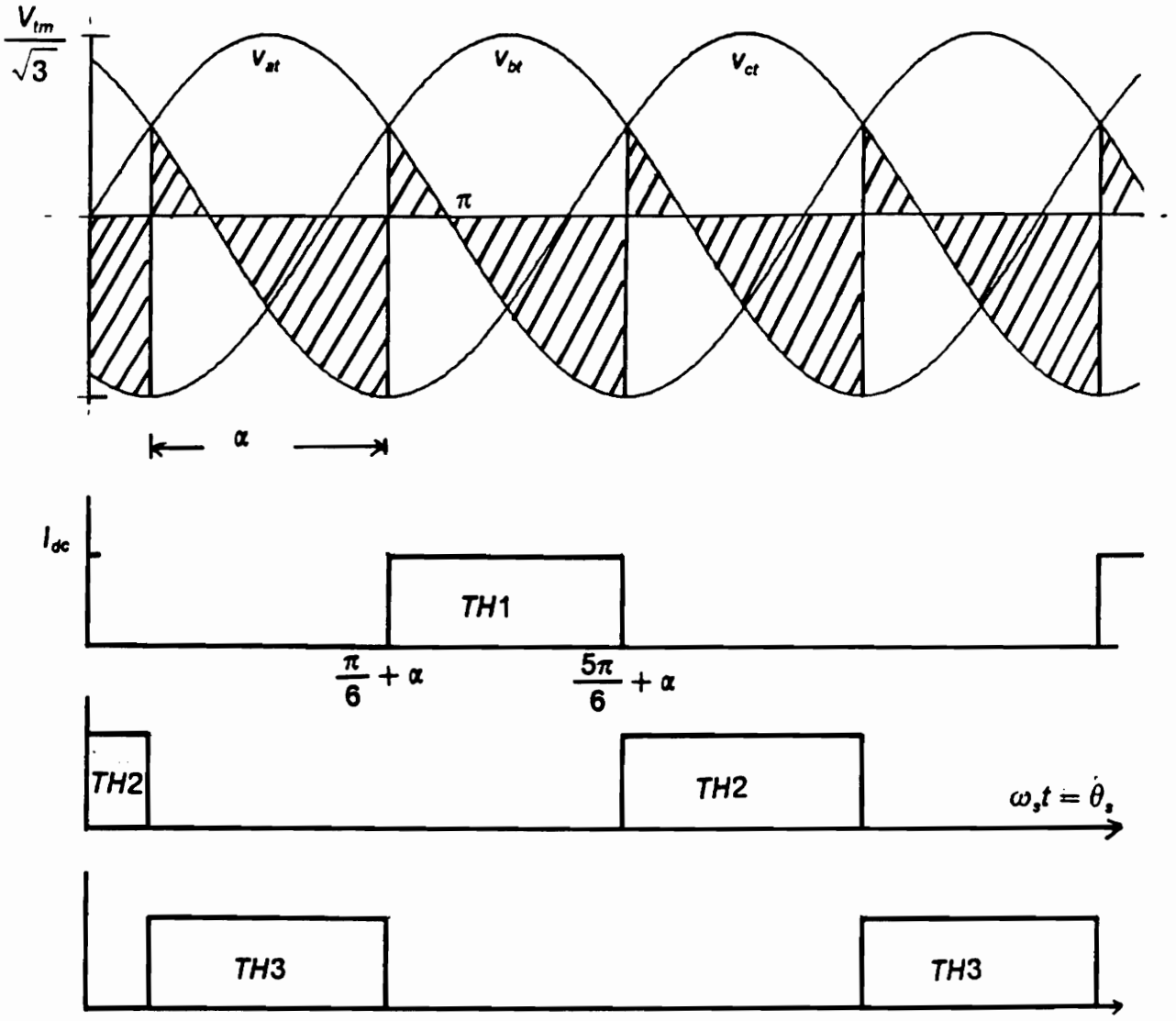

Figure 2.8 Waveforms of three phase half wave inverter:
(a) Phase voltage of the inverter ;
(b) Line current of the inverter ac side ;

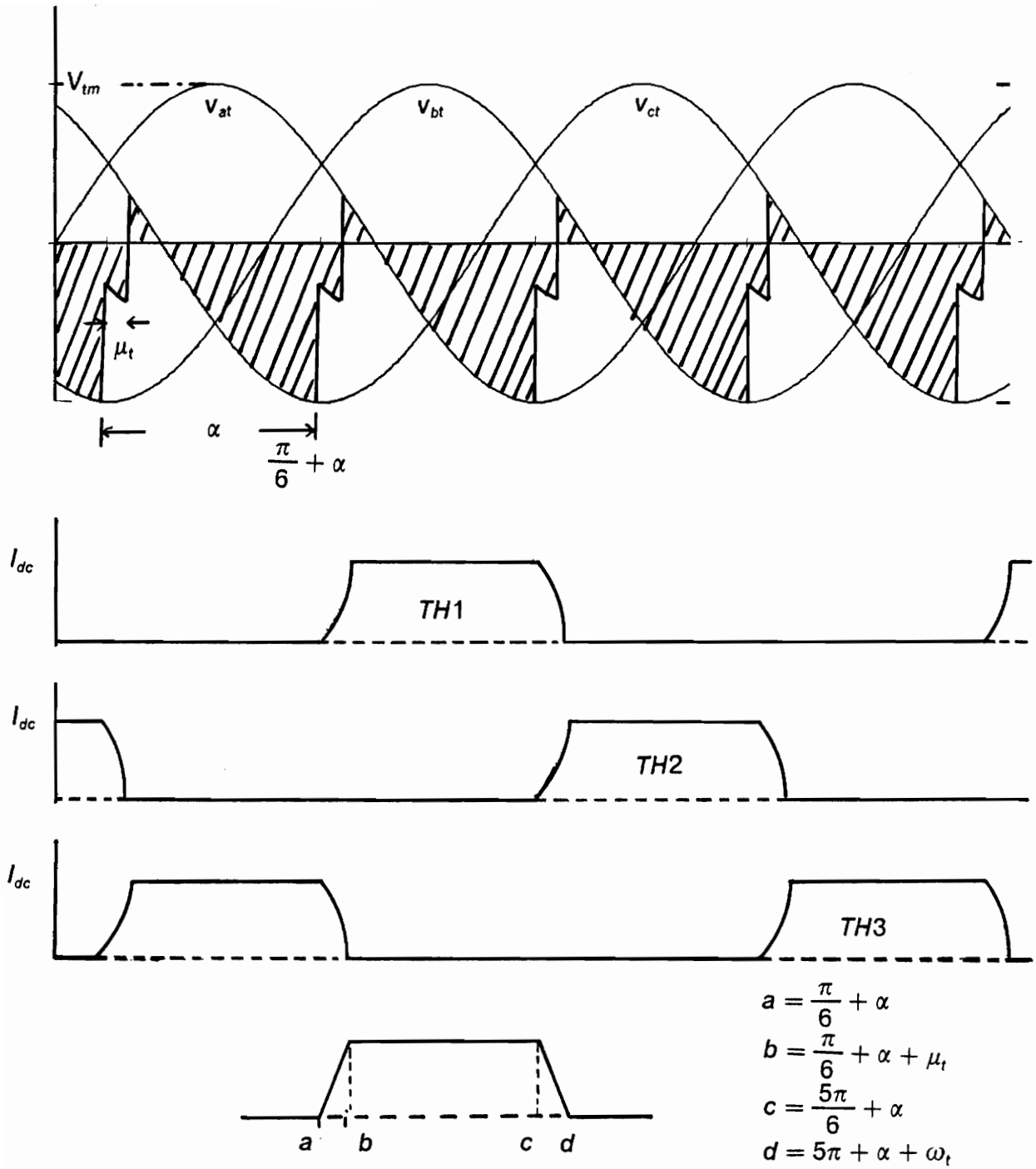

Figure 2.9 Waveforms of three phase half wave inverter with overlap:
(a) Phase voltage of the inverter;
(b) Line current of the inverter ac side;

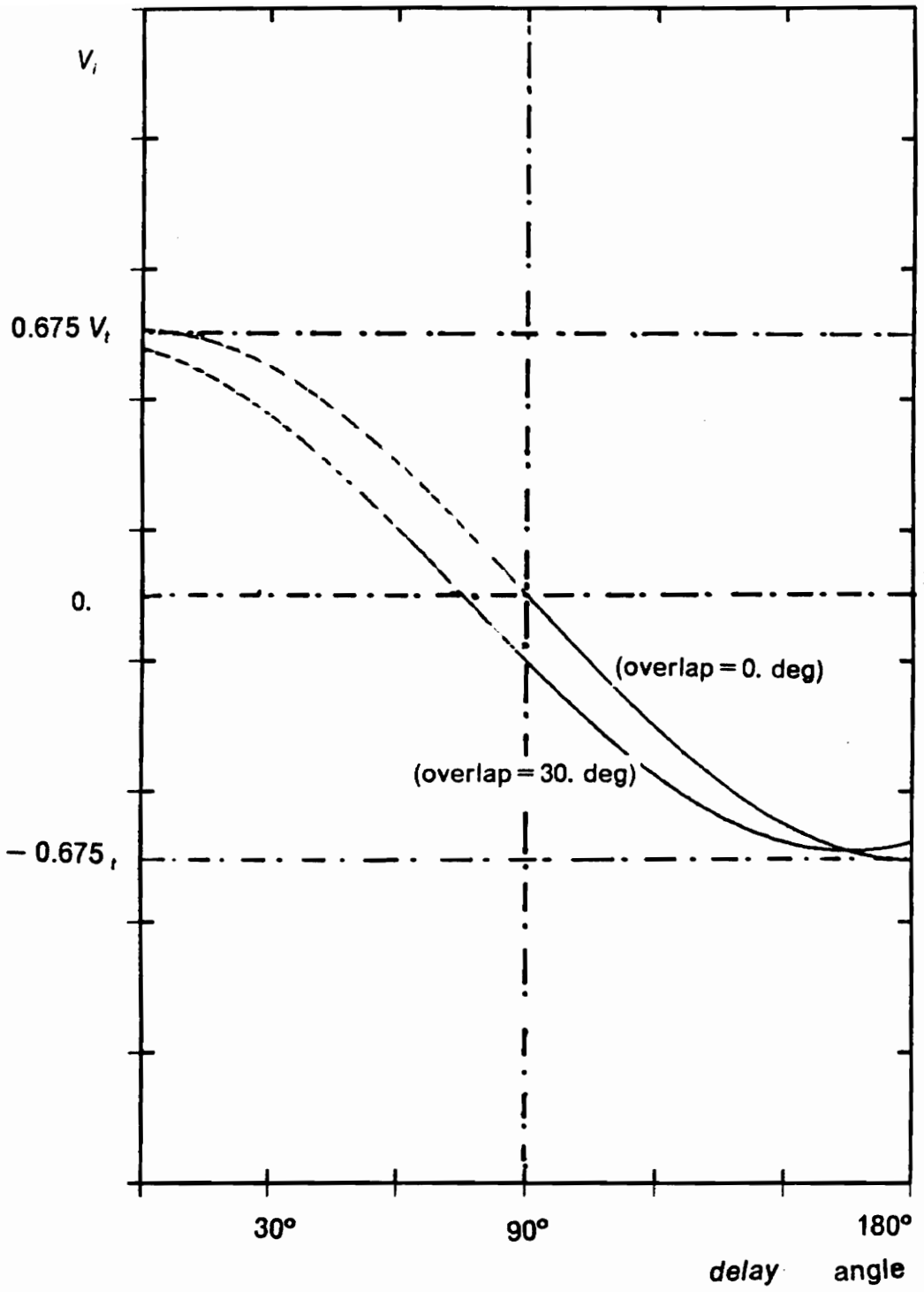

Figure 2.10 The inversion characteristics of THWI

$$
\begin{aligned}
i_{dc1}(t) &= \frac{\sqrt{3}\, I_{dc}}{\pi}(-\sin\alpha\ \cos\omega_s t + \cos\alpha\ \sin\omega st) \\
&= \frac{\sqrt{3}\, I_{dc}}{\pi}\sin(\omega_s t - \alpha)
\end{aligned}
\tag{2.42}
$$

Hence, the rms value of the fundamental current is

$$
I_{dc1} = \frac{\sqrt{3}\, I_{dc}}{\sqrt{2}\,\pi} \tag{2.43}
$$

The real power and reactive power can be represented by

$$
\begin{aligned}
P_0 &= \sqrt{3}\, V_t\, I_{dc1} \cos\alpha \\
&= \frac{3}{\sqrt{2}\,\pi} V_t\, I_{dc} \cos\alpha \\
&= V_i\, I_{dc}
\end{aligned}
\tag{2.44}
$$

$$
Q_0 = \frac{3}{\sqrt{2}\,\pi} V_t\, I_{dc}\ \sin\alpha \tag{2.45}
$$

where P_0 and Q_0 are the real and reactive power, respectively.

When the thyristors are triggered, there is an overlap due to the transformer reactance similar to the PMSG equivalent reactance on the rectifier bridge operation.

For the transformer equivalent reactance X_t per phase, the voltage lost due to the overlap is

$$
\begin{aligned}
V_{OL} &= \frac{3}{2\pi}\int_{\frac{\pi}{6}}^{\frac{\pi}{6}+\mu_t} v_{ct} - \frac{1}{2}(v_{ct}+v_{bt})d\omega_s t \\
&= \frac{3}{4\pi}\int_{\frac{\pi}{6}}^{\frac{\pi}{6}+\mu_t} \frac{V_{tm}}{\sqrt{3}}\{\sin(\omega_s t - \frac{2\pi}{3})\}d\omega_s t \\
&= \frac{3}{4\pi}\{\cos(\frac{\pi}{3}-\mu_t) - \frac{1}{2}\} \\
&= X_t I_{dc} \qquad (X_t = 2\pi f_s L_t)
\end{aligned}
\tag{2.46}
$$

from which the overlap angle μ_t is

$$
\mu_t = \frac{\pi}{3} - \cos^{-1}(\frac{1}{2} + \frac{4\pi}{3}\frac{I_{dc}}{V_{tm}}X_t) \tag{2.47}
$$

The line current with overlap angle, μ_t can be expressed by a Fourier series. For convenience of calculation, the wave form is assumed to be trapezoidal.

$$
i_{dc}(t) = \frac{a_0}{2} + \sum_{n=1}^{\infty}(a_n \cos\ n\theta_s + b_n \sin\ n\theta_s) \tag{2.48}
$$

where

$$
a_0 = \frac{4}{3}I_{dc} \tag{2.49}
$$

$$
\begin{aligned}
a_n = \frac{I_{dc}}{\pi}\frac{1}{n^2\mu_t}[&\cos\ n(\frac{\pi}{6}+\alpha+\mu_t) - \\
&\cos\ n(\frac{\pi}{6}+\alpha) + \cos\ n(\frac{5\pi}{6}) - \cos\ n(\frac{5\pi}{6}+\alpha+\mu_t)]
\end{aligned}
\tag{2.50}
$$

$$b_n = \frac{I_{dc}}{\pi}\frac{1}{n^2\mu_t}[\sin\ n(\frac{\pi}{6}+\alpha+\mu_t)\ - \\ \sin\ n(\frac{\pi}{6}+\alpha)+\sin\ n(\frac{5\pi}{6})-\sin\ n(\frac{5\pi}{6}+\alpha+\mu_t)] \tag{2.51}$$

The voltage transfer characteristic can be derived as the following:

$$\begin{aligned} V_i &= \frac{1}{\frac{2\pi}{3}}\int_{\pi+\alpha}^{\frac{\pi}{6}+\alpha+\mu_t}\frac{1}{2}(v_{at}+v_{ct})\,d\,\omega_s t+\int_{\frac{\pi}{6}+\alpha+\mu_t}^{\frac{5\pi}{6}+\alpha} v_{at}\,d\,\omega_s t \\ &= \frac{3}{2\pi}\frac{V_{tm}}{\sqrt{3}}[\int_{\frac{\pi}{6}+\alpha}^{\frac{\pi}{6}+\alpha+\mu_t}\frac{1}{2}\{\sin\omega_s t+\sin(\omega_s t+\frac{2\pi}{3})\}+\int_{\frac{\pi}{6}+\alpha+\mu_t}^{5\frac{\pi}{6}+\alpha}\sin\omega_s t\,d\,\omega_s t] \\ &= \frac{\sqrt{3}\,V_{tm}}{2\pi}[\frac{\sqrt{3}}{2}\cos\alpha+\frac{\sqrt{3}}{2}\cos(\alpha+\mu_t)] \\ &= \frac{\sqrt{6}}{2\pi}V_t[\frac{\sqrt{3}}{2}\cos\alpha+\frac{\sqrt{3}}{2}\cos(\alpha+\mu_t)] \end{aligned} \tag{2.52}$$

Considering the overlap angle due to the transformer equivalent reactance, the power can be calculated using the above results. The real and the reactive power are, respectively,

$$\begin{aligned} P_0 &= V_i I_{dc} \\ &= \frac{\sqrt{3}}{\sqrt{2}\,\pi}[\frac{\sqrt{3}}{2}\cos\alpha+\frac{\sqrt{3}}{2}\cos(\alpha+\mu_t)]V_t I_{dc} \end{aligned} \tag{2.53}$$

$$Q_0 = V_i I_{dc}\tan\alpha \tag{2.54}$$

2.6.2 Three phase full-wave inverter

A three phase full wave inverter scheme is shown in figure 2.11 and its voltage and current neglecting the overlap due to the transformer reactance are shown in figure 2.12.

The voltage at the output of the converter is

$$\begin{aligned} V_i &= \frac{1}{\frac{\pi}{3}} \int_{\frac{\pi}{6}}^{\frac{\pi}{2}} v_{at} - v_{bt}\, d\,\theta_s \\ &= \frac{3}{\pi} \int_{\frac{\pi}{6}}^{\frac{\pi}{2}+\alpha} \frac{V_{tm}}{\sqrt{3}} \{ \sin\theta_s - \sin(\theta_s - 2\frac{\pi}{3}) \}\, d\,\theta_s \\ &= \frac{3V_{tm}}{\pi} \cos\alpha \\ &= \frac{3\sqrt{2}}{\pi} V_t \cos\alpha \\ &= 1.35\, V_t \cos\alpha \end{aligned} \tag{2.55}$$

The link current as a summation of fundamental and harmonics is

$$i_{dc}(t) = \frac{a_0}{2} + \sum_{n=1}^{\infty} (a_n \cos\ n\theta_s + b_n \sin\ \theta_s) \tag{2.55}$$

where

$$a_0 = 0. \tag{2.57}$$

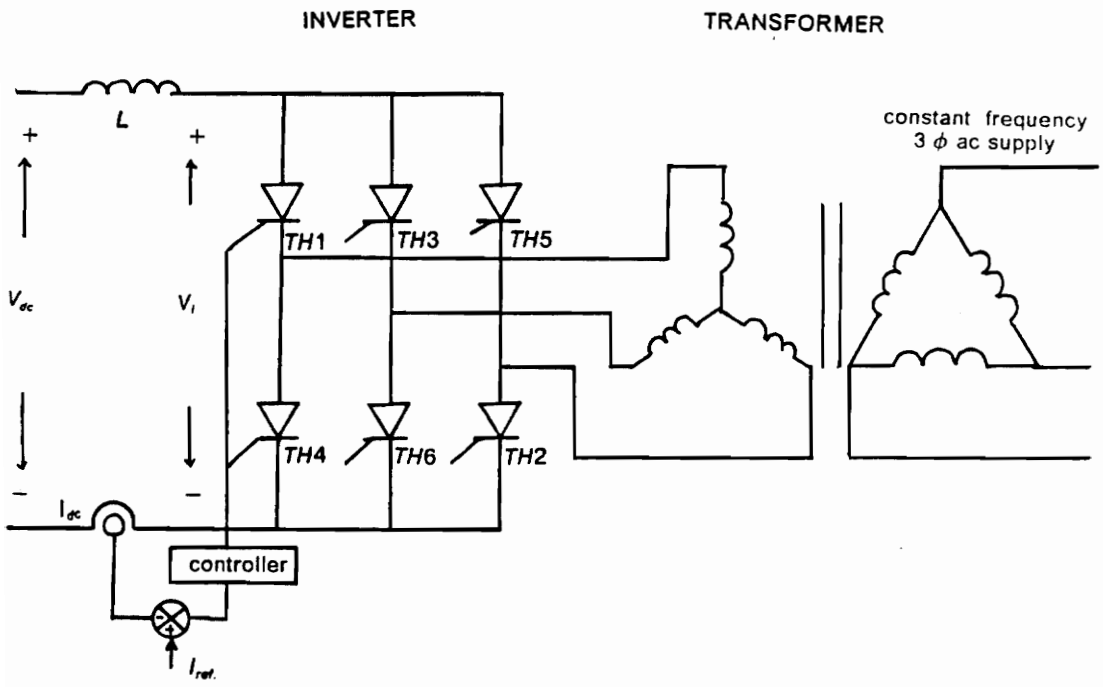

Figure 2.11 Three phase full-wave inverter

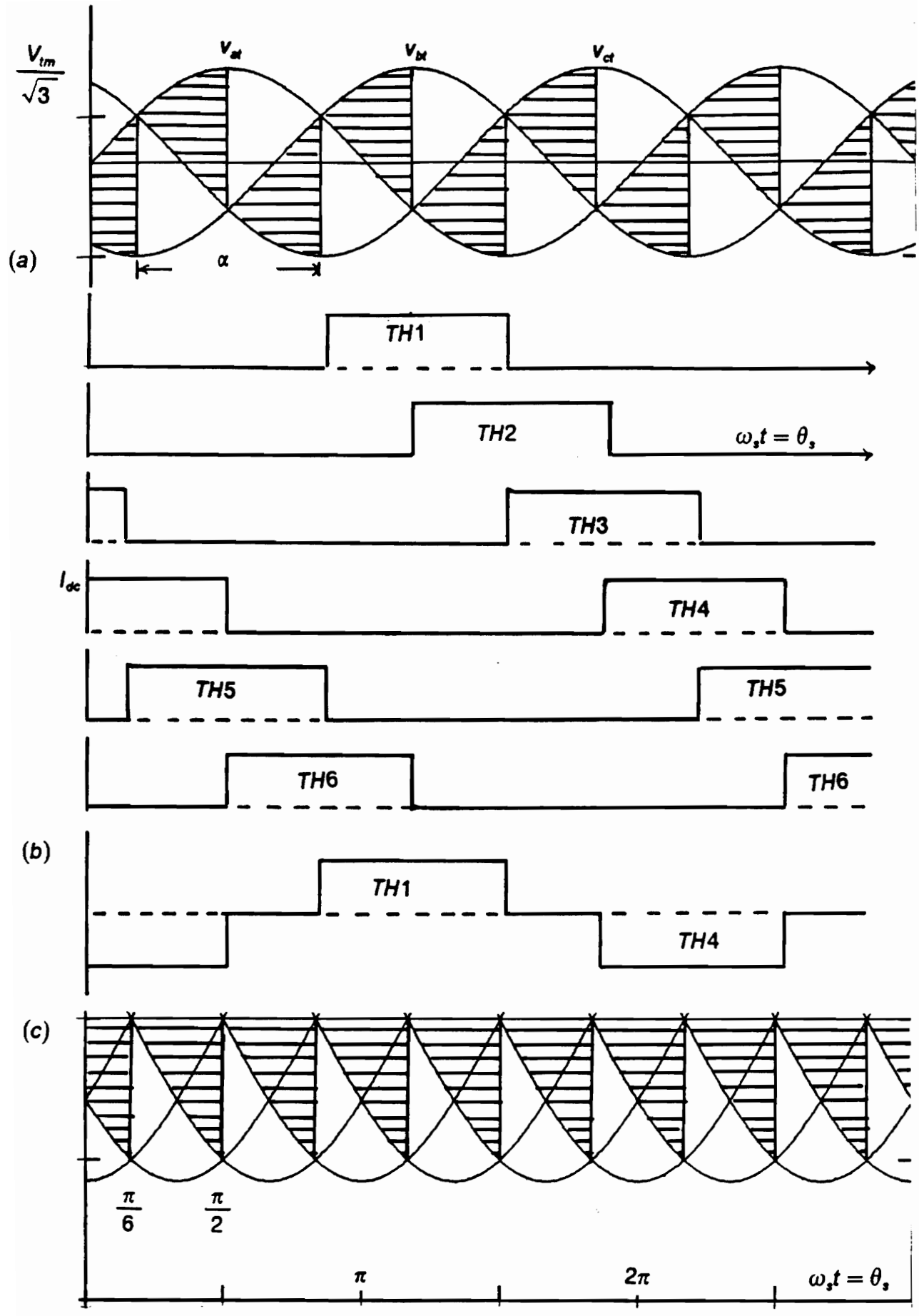

Figure 2.12 Waveforms of three phase full wave inverter:
(a) Phase voltage of the inverter;
(b) Line current of the inverter ac side ;

$$a_n = \frac{2I_{dc}}{\pi}\frac{1}{n}\left[\sin\ n\left(\frac{5\pi}{6}+\alpha\right) - \sin\ n\left(\frac{\pi}{6}+\alpha\right)\right] \tag{2.58}$$

$$b_n = \frac{2I_{dc}}{\pi}\frac{1}{n}\left[\sin\ n\left(\frac{5\pi}{6}+\alpha\right) - \sin\ n\left(\frac{\pi}{6}+\alpha\right)\right] \tag{2.59}$$

The fundamental component of current $i_{dc1}(t)$ is

$$i_{dc1}(t) = \frac{2\sqrt{3}\,I_{dc}}{\pi}\sin(\omega_s t - \alpha) \tag{2.60}$$

The rms value of the fundamental component current, I_{dc1} is

$$I_{dc1} = \frac{2\sqrt{3}\,I_{dc}}{\sqrt{2}\,\pi} \tag{2.61}$$

In the same way as in the half-wave inverter case, the real and the reactive power can be given as

$$\begin{aligned} P_0 &= \sqrt{3}\,V_t\,I_{dc1}\cos\alpha \\ &= \frac{6\cos\alpha}{\sqrt{2}\,\pi}V_t\,I_{dc} \\ &= V_i\,I_{dc} \end{aligned} \tag{2.62}$$

and

$$Q_0 = V_i\,I_{dc}\tan\alpha \tag{2.63}$$

respectively.

The overlap angle which affects the available voltage is to be calculated using the voltage difference during the overlap period is the same as the voltage applied to the transformer during this time.

$$
\begin{aligned}
V_{OL} &= \frac{3}{\pi}\int_{\frac{\pi}{6}}^{\frac{\pi}{6}+\mu_t} \frac{1}{2}(v_{ct} - v_{bt}) \\
&= \frac{3}{2\pi}\frac{V_{tm}}{\sqrt{3}}\int_{\frac{\pi}{6}}^{\frac{\pi}{6}+\mu_t} d\,\theta_s \\
&= \frac{3V_{tm}}{2\pi}[\cos(\frac{\pi}{3} - \mu_t) - \frac{1}{2}] \\
&= X_t\, I_{dc}
\end{aligned}
\tag{2.64}
$$

Hence, the overlap angle μ_t is

$$
\mu_t = \frac{\pi}{3} - \cos^{-1}[\frac{1}{2} + \frac{2\pi}{3}\frac{x_t I_{dc}}{V_{tm}}] \tag{2.65}
$$

The waveforms of the full-wave inverter with an overlap are shown in figure 2.13. The inverted dc link voltage is

$$
V_i = \frac{3\sqrt{2}\,V_t}{2\pi}\,[\cos\alpha + \cos(\alpha + \mu)] \tag{2.66}
$$

On the other hand, the actual current waveform in the inversion mode with overlap is not a rectangular waveform anymore. This waveform can similary be represented by equations (2.29) and (2.33). However, a trapezoidal current waveform is assumed for the present calculation.

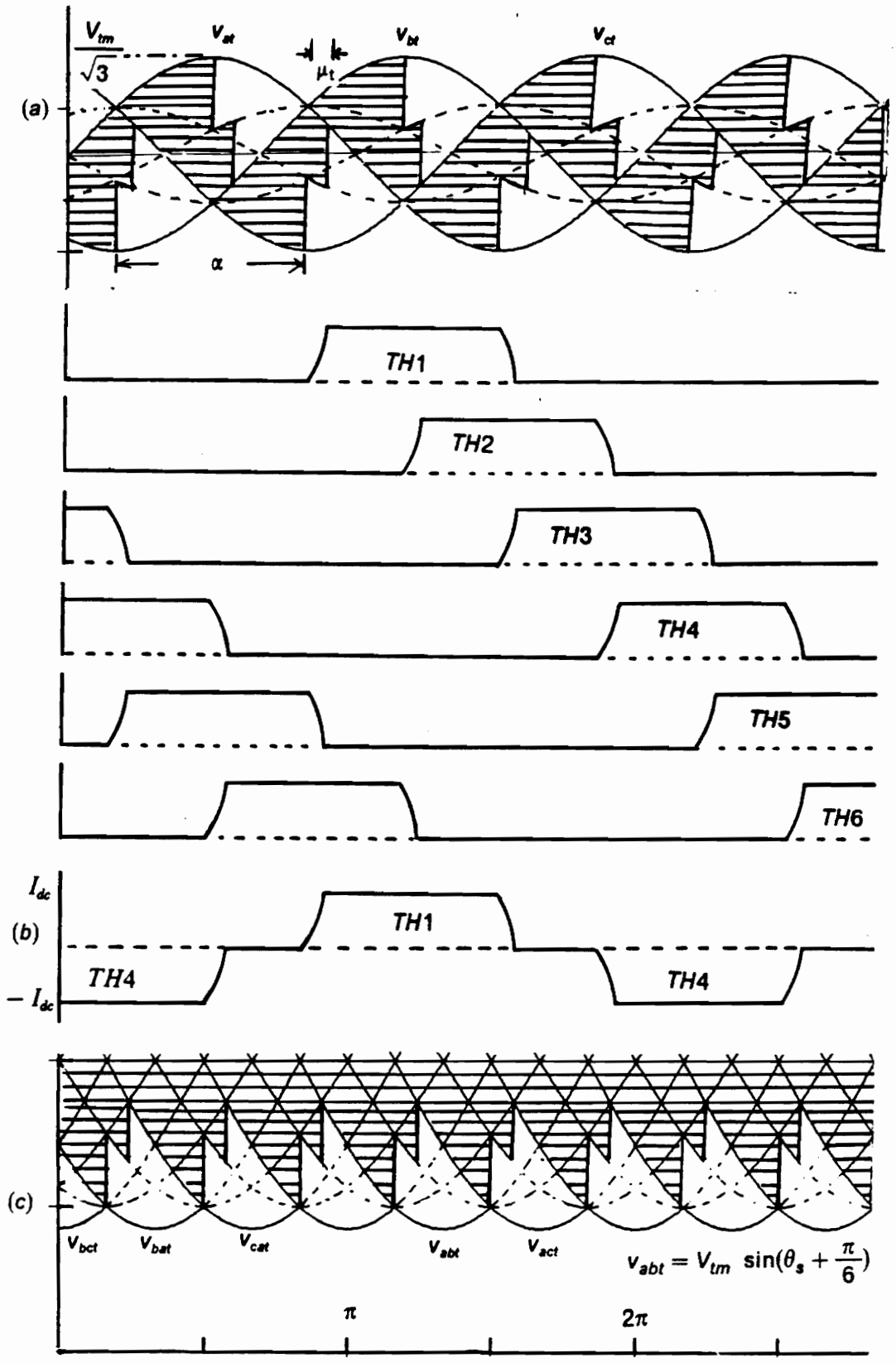

Figure 2.13 Waveforms of three phase full wave inverter with overlap:
(a), (c) Phase voltage of the inverter;
(b) Line current of the inverter ac side;

$$i_{dc}(t) = \frac{a_0}{2} + \sum_{n=1}^{\infty}(a_n \cos\ n\theta_s + b_n\ \sin\ n\theta_s) \tag{2.67}$$

where

$$a_0 = 0. \tag{2.68}$$

$$\begin{aligned} a_n = \frac{I_{dc}}{\pi}\frac{1}{n^2\mu_t}\ [&\cos\ n(\tfrac{\pi}{6}+\alpha+\mu) - \cos\ n(\tfrac{\pi}{6}+\alpha) - \cos(\tfrac{5\pi}{6}+\alpha+\mu_t) + \\ &\cos(\tfrac{5\pi}{6}+\alpha) + \cos\ n(\tfrac{7\pi}{6}-\alpha+\mu_t) + \cos\ n(\tfrac{7\pi}{6}+\alpha) - \\ &\cos\ n(\tfrac{11\pi}{6}+\alpha+\mu_t) + \cos\ n(\tfrac{11\pi}{6}+\alpha)] \end{aligned} \tag{2.69}$$

$$\begin{aligned} b_n = \frac{I_{dc}}{\pi}\frac{1}{n^2\mu_t}\ [&\sin\ n(\tfrac{\pi}{6}+\alpha+\mu) - \sin\ n(\tfrac{\pi}{6}+\alpha) - \sin(\tfrac{5\pi}{6}+\alpha+\mu_t) + \\ &\sin(\tfrac{5\pi}{6}+\alpha) + \sin\ n(\tfrac{7\pi}{6}+\alpha+\mu_t) + \sin\ n(\tfrac{7\pi}{6}+\alpha) + \\ &+ \sin\ n(\tfrac{11\pi}{6}+\alpha+\mu_t) - \sin\ n(\tfrac{11\pi}{6}+\alpha)] \end{aligned} \tag{2.70}$$

Using the above I_{dc} and V_i values, the active and the reactive power are respectively obtained:

$$P_0 = V_i\ I_{dc} \tag{2.71}$$

$$Q_0 = V_i\ I_{dc} \tan\alpha \tag{2.72}$$

The characteristic relationship between the controlled angle and the inverter voltage is shown in figure 2.14.

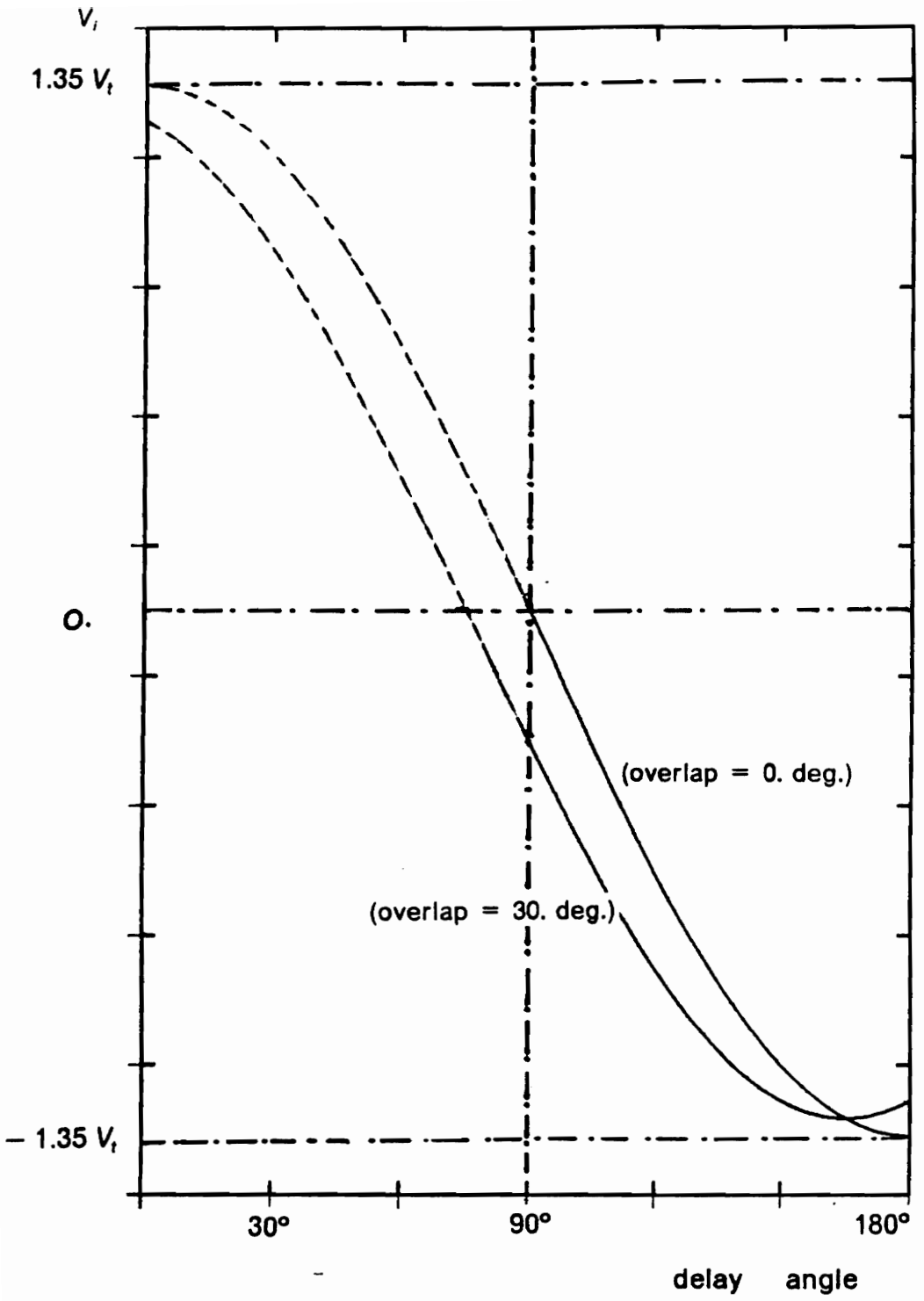

Figure 2.14 The inversion characteristic of TFWI

2.7 Losses and overall efficiency

This section cosiders the losses and overall efficiency of the VSCF power conversion scheme. PM machines have a varying efficiency over the speed range. As shown in equation (2.2), the machine equivalent resistance observed on the stator terminal is a function of d, q-axes reactance, which means that the equivalent resistance of the machine is dependent on the machine speed. The equivalent machine resistance is as seen from equations (2.2). Therefore at higher speed, the machine has a higher equivalent resistance, which results in a relatively lower overall efficiency at the rated speed.

The diode-rectifier bridge has 6 diodes and each diode has a static resistance. The static resistance varies widely with the applied voltage and current and has a non-linear relationship.

The overall efficiency including the device-losses is

$$\begin{aligned}\eta &= \frac{Output\ Power}{Generated\ Power} \\ &= \frac{P_o}{P_{in}} \\ &= \frac{I_{dc}\, V_l}{3\, I_{g1}^2\, R_{eq} + P_{Dl} + P_{RE} + I_{dc}\, V_l}\end{aligned} \tag{2.73}$$

where I_{g1} is the fundamental component of I_{dc} , $I_{g1}^2 R_{eq}$ is the PMSG loss per phase, P_{Dl} is the diode-bridge loss and P_{RE} is the reactor loss

Chpter 3. Harmonics

3.1 Introduction

This chapter covers the harmonics generated from ac to dc on the PMSG side or dc to ac on the controlled converter side. Here, harmonics are defined as voltage and current that are present in this scheme as integral multiples of 60 Hz or the generated-voltage frequency. The waveforms of the current (ac side) and the voltage (dc side) are analyzed on both sides of the rectifier and inverters using a Fourier series.

3.2 Preliminary on Fourier series

A periodic function can be expressed as a trigonometric series using Fourier series. If a periodic function $f(\theta)$ has a period of 2π, $f(\theta)$ can be represented as,

$$f(\theta) = \frac{a_0}{2} + \sum_{n=1}^{\infty} (a_n \cos\ n\theta + b_n \sin\ n\theta) \tag{3.1}$$

where

$$a_0 = \frac{1}{\pi} \int_0^{2\pi} f(\theta)\, d\,\theta \tag{3.2}$$

$$a_n = \frac{1}{\pi} \int_0^{2\pi} f(\theta)\ \cos\ n\theta\, d\theta \tag{3.3}$$

$$b_n = \frac{1}{\pi} \int_0^{2\pi} f(\theta)\ \sin\ n\theta\, d\theta \tag{3.4}$$

Alternatively, $f(\theta)$ can be written as

$$f(\theta) = \frac{a_0}{2} + \sum_{n=1}^{\infty} c_n \cos(\, n\theta + \phi) \tag{3.5}$$

where

$$c_n = \sqrt{a_n^2 + b_n^2} \tag{3.6}$$

$$\phi_n = \tan^{-1} \frac{b_n}{a_n} \tag{3.7}$$

where c_n , ϕ_n are the magnitude and phase angle of the n^{th} harmonic, respectively.

3.3 Harmonics generated by diode-bridge rectifier

The ideal case of the three phase full wave rectifier waveforms are shown in figure 2.12 (b) and (c) . Since the waveforms have a period of 2π , equation (3.1) can be used for the waveform representation.

The line current $i_g(\theta_r)$ is

$$i_g(\theta_r) = \frac{a_0}{2} + \sum (a_n \cos n\theta_r + b_n \sin n\theta_r) \tag{3.8}$$

where

$$\theta_r = \omega_r t \tag{3.9}$$

$$a_0 = 0. \tag{3.10}$$

$$a_n = 0. \tag{3.11}$$

$$\begin{aligned} b_n &= \frac{I_{dc}}{\pi}\int_{\frac{\pi}{6}}^{\frac{5\pi}{6}} \sin n\theta_r \, d\theta - \int_{\frac{7\pi}{6}}^{\frac{11\pi}{6}} \sin n\theta_r \, d\theta_r \\ &= \frac{I_{dc}}{\pi}\frac{1}{n}\left[\cos\frac{n\pi}{6} - \cos\frac{5n\pi}{6} - \cos\frac{7n\pi}{6} + \cos\frac{11n\pi}{6} + \; - \; ...\right] \end{aligned} \tag{3.12}$$

Hence,

$$i_g(\theta_r) = \frac{2\sqrt{3}\, I_{dc}}{\pi}\left(\sin\theta_r - \frac{1}{5}\sin 5\theta_r - \frac{1}{7}\sin 7\theta_r + \frac{1}{11}\sin 11\theta_r + \; - \right) \tag{3.13}$$

The rms value of the generator line current is

$$I_{rms} = \sqrt{\frac{1}{2\pi}\int_0^{2\pi} i^2(\theta_r)\, d\theta_r}$$
$$= \sqrt{\frac{1}{\pi}\int_{\frac{\pi}{6}}^{\frac{5\pi}{6}} I_{dc}^2\, d\theta_r} \qquad (3.14)$$
$$= \sqrt{\frac{2}{3}}\, I_{dc}$$

and the rms value of the fundamental component of the line current is

$$I_{rms1} = \frac{\sqrt{6}}{\pi} I_{dc} \qquad (3.15)$$

Hence, the rms value of the total harmonic current is

$$I_{rmsh} = \sqrt{I_{rms}^2 - I_{rms1}^2}$$
$$= \sqrt{\frac{2}{3} - \frac{6}{\pi^2}}\; I_{dc} \qquad (3.16)$$
$$= 0.242\, I_{dc}$$

Since the voltage waveform on the dc side has a period of $\frac{\pi}{3}$, the dc output voltage can be expressed as

$$v_{dc}(\theta_r) = \frac{a_0}{2} + \sum_{n=1}^{\infty}(a_n \cos 6n\theta_r + b_n \sin 6n\theta_r) \qquad (3.17)$$

If the waveform is referred to the orign o o′, then

$$a_0 = \frac{6}{\pi}\int_{-\frac{\pi}{6}}^{\frac{\pi}{6}} V_{gm} \cos \theta_r\, d\theta_r$$
$$= \frac{6\sqrt{2}}{\pi} V_g \qquad (3.18)$$

$$a_n = \frac{6}{\pi}\int_{-\frac{\pi}{6}}^{\frac{\pi}{6}} V_{gm} \cos\theta_r \cos 6n\theta_r \, d\theta_r$$

$$= \frac{3\sqrt{2}\,V_g}{\pi}\left[\frac{2}{1-6n}\sin(1-6n)\frac{\pi}{6} + \frac{2}{1+6n}\sin(1+6n)\frac{\pi}{6}\right] \tag{3.19}$$

$$= \frac{6\sqrt{2}\,V_g}{\pi}\,\frac{(-1)^n}{1-36n^2}$$

$$b_n = 0. \tag{3.20}$$

The dc output voltage is then,

$$v_{dc}(\theta_r) = \frac{3\sqrt{2}\,V_g}{\pi}\left[1 + 2\sum_{n=1}^{\infty}\frac{(-1)^n}{1-36n^2}\cos 6n\theta_r\right] \tag{3.21}$$

Hence, the dc average voltage, V_{dc}, is

$$V_{dc} = \frac{3\sqrt{2}}{\pi}V_g \tag{3.22}$$

Consequently, a three-phase full-wave rectifier principally generates the order of $6n\pm1$ harmonic currents on ac side, and the order of $6n$ harmonic voltages on the dc link side, where n is an integer.

The orders of harmonics mentioned above are for the ideal converter but, the actual conversion mode produces all orders of harmonics which are caused by the unbalanced ac source, the overlap angle, non-ideal switching devices, non-ideal switching characteristics, etc.

If a symmetrical machine, balanced ac sinusoidal source voltage and ideal switching devices are assumed, the overlap angle mainly affects the harmonics of the ideal conversion. Consequently, it is important to analyze the harmonics with the overlap angle being considered. In this analysis, the overlap angle is assumed to be less than 60° and the current waveform is assumed to be trapezoidal for simplicity. The waveforms of the current and voltage are shown in figure 2.5 with the hatched area being considered.

The line current is

$$i(\theta_r) = \frac{a_0}{2} + \sum_{n=1}^{\infty} (a_n \cos n\theta_r + b_n \sin n\theta_r) \tag{3.23}$$

where

$$a_0 = 0. \tag{3.24}$$

$$a_n = 0. \tag{3.25}$$

If the current waveform is referred to the origin o o′, then

$$b_n = \frac{2}{\pi}\left[\int_a^b \frac{I_{dc}}{\mu}(\theta_r - a)\ \sin\ n\theta_r\, d\theta_r + \int_b^c I_{dc}\ \sin\ n\theta_r\, d\theta_r + \int_c^d -\frac{I_{dc}}{\mu}(\theta_r - d)\ \sin\ n\theta_r\, d\theta_r\right]$$

$$= \frac{2I_{dc}}{\pi}\frac{1}{n}\left[\cos\ nb - \cos\ nc + \frac{1}{\mu}(a\cos\ na - b\cos nb + c\ \cos nc - d\cos nd) + \frac{1}{n\mu}(\sin\ nb - \sin\ na + \sin\ nd - \sin\ nc)\right] \tag{3.26}$$

$$= \frac{2I_{dc}}{\pi}\frac{1}{n}\left[\cos\ n(\frac{\pi}{6}+\mu) - \cos\frac{5n\pi}{6} + \frac{1}{\mu}\{\frac{\pi}{6}\cos\frac{n\pi}{6} - (\frac{\pi}{6}+\mu)\cos\ n(\frac{\pi}{6}+\mu) + \frac{5\pi}{6}\cos\frac{5n\pi}{6} - (\frac{5\pi}{6}+\mu)\cos\ n(\frac{5\pi}{6}+\mu)\} + \frac{1}{n\mu}\{\sin\ n(\frac{\pi}{6}+\mu) - \sin\frac{n\pi}{6} + \sin\ n(5\frac{\pi}{6}+\mu) - \sin\frac{5n\pi}{6}\}\right]$$

That is,

$$i_{(\theta_r)} = \sum_{n=1}^{\infty} b_n \frac{\sin\ n\theta_r}{n} \tag{3.27}$$

If the voltage is expressed in a similar way to that of the ideal case, the dc output voltage is

$$v_{dc} = \frac{a_0}{2} + \sum_{n=1}^{\infty}(a_n\cos\ n\theta_r + b_n\ \sin\ n\theta_r) \tag{3.28}$$

If the voltage waveform is referred to the origin o o′, then,

$$a_0 = \frac{6}{\pi}\left[\int_{-\frac{\pi}{6}}^{\frac{\pi}{6}} V_{gm}\cos\theta_r\, d\theta_r - \frac{V_{gm}}{2}\int_{-\frac{\pi}{6}}^{-\frac{\pi}{6}+\mu} \cos\theta_r - \cos(\theta_r+\frac{\pi}{3})\, d\theta_r\right]$$
$$= \frac{6\sqrt{2}\,V_g}{\pi}\left[\frac{1}{2}+\frac{1}{2}\{\sin(\frac{\pi}{6}+\mu)+\sin(\frac{\pi}{6}-\mu)\}\right] \tag{3.29}$$

$$a_n = \frac{6}{\pi}\left[\int_{-\frac{\pi}{6}}^{\frac{\pi}{6}} V_{gm}\cos\theta_r\cos 6n\theta_r d\theta_r - \int_{-\frac{\pi}{6}}^{-\frac{\pi}{6}+\mu}\frac{V_{gm}}{2}\{\cos\theta_r-\cos(\theta_r+\frac{\pi}{3})\}\cos 6n\theta_r\, d\theta_r\right]$$
$$= \frac{3\sqrt{2}\,V_g}{\pi}\left[\frac{2}{1-6n}\{3\sin(1-6n)\frac{\pi}{6}-\frac{1}{2}\sin((1-6n)(\frac{\pi}{6}-\mu)-\frac{\pi}{3})+\right.$$
$$\frac{1}{2}\sin((1-6n)\frac{\pi}{6}-\frac{\pi}{3})+\sin(1-6n)(\frac{\pi}{6}-\mu)\}+$$
$$\frac{2}{(1+6n)}\{3\sin(1+6n)\frac{\pi}{6}-\frac{1}{2}\sin((1+6n)(\frac{\pi}{6}-\mu)-\frac{\pi}{3})+$$
$$\left.\frac{1}{2}\sin((1+6n)\frac{\pi}{6}-\frac{\pi}{3})+\sin(1+6n)(\frac{\pi}{6}-\mu)\}\right] \tag{3.30}$$

And

$$v_{dc} = \frac{3\sqrt{2}\,V_g}{\pi}\{\frac{1}{2}-\sin(\mu-\frac{\pi}{6})+\sum_{n=1}^{\infty} a_n\cos 6n\,\theta_r\} \tag{3.31}$$

Hence, the average dc voltage is:

$$V_{dc} = \frac{3\sqrt{2}\,V_g}{\pi}\left[\frac{1}{2}+\frac{1}{2}\{\sin(\frac{\pi}{6}+\mu)+\sin(\frac{\pi}{6}-\mu)\}\right] \tag{3.32}$$

3.4 Harmonics generated by inverters

In this section, the harmonics generated by the controlled converter in the inversion mode are analyzed. Its variation with respect to the triggering angle is quantified.

3.4.1 Three-phase half-wave inverter

The voltage and the current waveforms of the three-phase half-wave inverter, neglecting the overlap angle, are shown in figure 2.8. The conduction angle for the SCR is $\frac{2\pi}{3}$. Accordingly, the current can be expressed as in equation (3.1).

$$i(t) = \frac{a_0}{2} + \sum_{n=1}^{\infty} (a_n \cos n\theta_s + b_n \sin n\theta_s) \tag{3.33}$$

where

$$\theta_s = \omega_s t \tag{3.34}$$

$$\begin{aligned} a_0 &= \frac{1}{\pi} \int_{\frac{\pi}{6}+\alpha}^{\frac{5\pi}{6}+\alpha} I_{dc}\, d\theta_s \\ &= \frac{2}{3} I_{dc} \end{aligned} \tag{3.35}$$

$$a_n = \frac{1}{\pi}\int_{\frac{\pi}{6}+\alpha}^{\frac{5\pi}{6}} I_{dc} \cos n\theta_s \, d\theta_s$$
$$= \frac{I_{dc}}{\pi}\frac{1}{n}\left[\sin n\left(\frac{5\pi}{6}+\alpha\right) - \sin n\left(\frac{\pi}{6}+\alpha\right)\right] \tag{3.36}$$

$$b_n = \frac{1}{\pi}\int_{\frac{\pi}{6}+\alpha}^{\frac{5\pi}{6}+\alpha} I_{dc} \sin n\theta_s d\theta_s$$
$$= \frac{I_{dc}}{\pi}\frac{1}{n}\left[-\cos n\left(\frac{5\pi}{6}+\alpha\right) + \cos n\left(\frac{\pi}{6}+\alpha\right)\right] \tag{3.37}$$

Hence, the rms value of the line current and its fundamental component are, respectively:

$$I_{rms} = \sqrt{\frac{1}{2\pi}\int_0^{2\pi} i^2(\theta_s)\, d\theta_s}$$
$$= \frac{1}{\sqrt{3}} I_{dc} \tag{3.38}$$

$$I_{rms1} = \frac{1}{\sqrt{2}}\sqrt{a_1^2 + b_1^2}$$
$$= \sqrt{\frac{3}{2}}\frac{1}{\pi} I_{dc} \tag{3.39}$$

The magnitude of the n^{th} harmonic is

$$c_n = \sqrt{a_n^2 + b_n^2}$$
$$= \frac{I_{dc}}{\pi}\frac{1}{n}\cos\frac{2n\pi}{3} \tag{3.40}$$

indicating that the magnitude of the harmonics is independent of α.

As for its voltage output it can be expressed as

$$v_i(\theta_s) = \frac{a_0}{2} + \sum_{n=1}^{\infty}(a_n \cos\ n\theta_s + b_n \sin\ n\theta_s) \tag{3.41}$$

where

$$\begin{aligned} a_0 &= \frac{2}{\frac{2\pi}{3}} \int_{\frac{\pi}{6}+\alpha}^{\frac{5\pi}{6}+\alpha} \frac{V_{tm}}{\sqrt{3}} \sin\ \theta_s\, d\theta_s \\ &= \frac{3\sqrt{2}}{3} V_t \cos\ \alpha \end{aligned} \tag{3.42}$$

$$\begin{aligned} a_n &= \frac{3}{\pi} \int_{\frac{\pi}{6}+\alpha}^{\frac{5\pi}{6}+\alpha} \frac{V_{tm}}{\sqrt{3}} \sin\theta_s \cos\ 3n\,\theta_s\, d\theta_s \\ &= \frac{\sqrt{6}\ V_t}{2\pi}\left[\frac{1}{1-3n}\left\{-\cos\ (1-3n)\left(\frac{5\pi}{6}+\alpha\right) + \cos\ (1-3n)\left(\frac{\pi}{6}+\alpha\right)\right\} + \right. \\ &= \left. \frac{1}{1+3n}\left\{-\cos\ (1+3n)\left(\frac{5\pi}{6}+\alpha\right) + \cos\ (1+3n)\left(\frac{\pi}{6}+\alpha\right)\right\}\right] \end{aligned} \tag{3.43}$$

$$\begin{aligned} b_n &= \frac{3}{\pi} \int_{\frac{\pi}{6}+\alpha}^{\frac{5\pi}{6}+\alpha} \frac{V_{tm}}{\sqrt{3}} \sin\theta_s \sin\ 3n\,\theta_s\, d\theta_s \\ &= \frac{\sqrt{6}\ V_t}{2\pi}\left[\frac{1}{1-3n}\left\{\sin\ (1-3n)\left(\frac{5\pi}{6}+\alpha\right) - \sin\ (1-3n)\left(\frac{\pi}{6}+\alpha\right)\right\} + \right. \\ &= \left. \frac{1}{1+3n}\left\{\sin\ (1+3n)\left(\frac{5\pi}{6}+\alpha\right) - \sin\ (1+3n)\left(\frac{\pi}{6}+\alpha\right)\right\}\right] \end{aligned} \tag{3.44}$$

In the final form, the inverter output voltage is

$$v_i(\theta_s) = \frac{3\sqrt{2}}{2\pi} V_t \cos \alpha + \sum_{n=1}^{\infty} (a_n \cos 3n\theta_s + b_n \sin 3n\theta_s) \tag{3.45}$$

Hence, the average dc value of the voltage V_i is

$$V_i = \frac{3\sqrt{2}}{2\pi} V_t \cos \alpha \tag{3.46}$$

The waveforms of voltage and current of a half wave inverter with overlap angle μ_t are shown in figure 2.9. The current has a period of 2π and its waveform is assumed to be trapezoidal as mentioned before.

The current $i_i(\theta_s)$ can be expressed as

$$i_i(\theta_s) = \frac{a_0}{2} + \sum_{n=1}^{\infty} (a_n \cos n\theta_s + b_n \sin n\theta_s) \tag{3.47}$$

where

$$a_0 = \frac{2}{3} I_{dc} \tag{3.48}$$

$$
\begin{aligned}
a_n &= I_{dc}\left[\int_a^b \frac{1}{\mu_t}(\theta_s - a)\ \cos\ n\theta_s + \int_b^c \cos\ n\theta_s - \int_c^d \frac{1}{\mu_t}(\theta_s - d)\ \cos\ n\theta_s\right]d\theta_s \\
&= \frac{I_{dc}}{\pi}\frac{1}{n^2\mu_t}(\cos\ nb - \cos\ na + \cos\ nc - \cos nd) \\
&= \frac{I_{dc}}{\pi}\frac{1}{n^2\mu_t}\left[\cos\ n\left(\frac{\pi}{6} + \alpha + \mu_t\right) - \cos\ n\left(\frac{\pi}{6} + \alpha\right) + \cos\ n\left(\frac{5\pi}{6} + \alpha\right) - \right. \\
&\quad \left. \cos\ n\left(\frac{5\pi}{6} + \alpha + \mu_t\right)\right]
\end{aligned}
\tag{3.49}
$$

$$
\begin{aligned}
b_n &= I_{dc}\left[\int_a^b \frac{1}{\mu_t}(\theta_s - a)\ \sin\ n\theta_s + \int_b^c \sin\ n\theta_s - \int_c^d \frac{1}{\mu_t}(\theta_s - d)\ \sin\ n\theta_s\right]d\theta_s \\
&= \frac{I_{dc}}{\pi}\frac{1}{n^2\mu_t}(\sin\ nb - \sin\ na + \sin\ nc - \sin nd) \\
&= \frac{I_{dc}}{\pi}\frac{1}{n^2\mu_t}\left[\sin\ n\left(\frac{\pi}{6} + \alpha + \mu_t\right) - \sin\ n\left(\frac{\pi}{6} + \alpha\right) + \sin\ n\left(\frac{5\pi}{6} + \alpha\right) - \right. \\
&\quad \left. \sin\ n\left(\frac{5\pi}{6} + \alpha + \mu_t\right)\right]
\end{aligned}
\tag{3.50}
$$

That is,

$$
i_i(t) = \frac{1}{3}I_{dc} + \sum_{n=1}^{\infty}(a_n\ \cos\ n\theta_s + b_n\ \sin\ n\theta_s) \tag{3.51}
$$

Similarly the inverter output voltage is

$$
v_i(\theta_s) = \frac{a_0}{2} + \sum_{n=1}^{\infty}(a_n\ \cos\ n\theta_s + b_n\ \sin\ n\theta_s) \tag{3.52}
$$

where

$$
\begin{aligned}
a_0 &= \frac{3}{\pi}\left[\int_a^b \frac{v_{at}+v_{ct}}{2} + \int_b^c v_{at}\right] d\theta_s \\
&= \frac{\sqrt{3}\,V_{tm}}{2\pi}\left[\cos\left(\frac{\pi}{6}+\alpha\right) + \cos\left(\frac{5\pi}{6}+\alpha\right) + \cos\left(\frac{\pi}{6}+\alpha+\mu_t\right) - \right. \\
&\quad \left. \cos\left(\frac{5\pi}{6}+\alpha+\mu_t\right) - 2\cos\left(\frac{5\pi}{6}+\alpha\right)\right] \\
&= \frac{3\sqrt{2}\,V_t}{2\pi}\left[\cos\left(\alpha+\mu_t\right) + \cos\,\alpha\right]
\end{aligned}
\tag{3.53}
$$

$$
\begin{aligned}
a_n &= \frac{3}{\pi}\left[\int_a^b \frac{v_{at}+v_{ct}}{2} + \int_b^c v_{at}\right] \cos 3n\theta_s d\theta_s \\
&= \frac{\sqrt{3}\,V_{tm}}{2\pi}\left[\int_a^b \left\{\sin\,\theta_s + \sin\left(\theta_s+\frac{2\pi}{3}\right)\cos\,3n\theta_s + \int_b^c 2\sin\,\theta_s\cos\,3n\theta_s\right] d\theta_s\right. \\
&= \frac{\sqrt{6}\,V_t}{4\pi}\left[\frac{1}{1-3n}\left\{\frac{1}{2}\cos\,(1-3n)\left(\frac{\pi}{6}+\alpha\right) - \frac{\sqrt{3}}{2}\sin\,(1-3n)\left(\frac{\pi}{6}+\alpha\right) + \right.\right. \\
&\quad \frac{3}{2}\cos\,(1-3n)\left(\frac{\pi}{6}+\alpha+\mu_t\right) + \\
&\quad \left.\frac{\sqrt{3}}{2}\sin\,(1-3n)\left(\frac{\pi}{6}+\alpha+\mu_t\right) - 2\cos\,(1-3n)\left(\frac{5\pi}{6}+\alpha\right)\right\} + \\
&\quad \frac{1}{1+3n}\left\{\frac{1}{2}\cos\,(1+3n)\left(\frac{\pi}{6}+\alpha\right) - \frac{\sqrt{3}}{2}\sin\,(1+3n)\left(\frac{\pi}{6}+\alpha\right) + \right. \\
&\quad \frac{3}{2}\cos\,(1+3n)\left(\frac{\pi}{6}+\alpha+\mu_t\right) + \frac{\sqrt{3}}{2}\sin\,(1+3n)\left(\frac{\pi}{6}+\alpha+\mu_t\right) \\
&\quad \left.\left.\left. -2\cos\,(1+3n)\left(\frac{5\pi}{6}+\alpha\right)\right\}\right]
\end{aligned}
\tag{3.54}
$$

$$
\begin{aligned}
b_n &= \frac{3}{\pi}\left[\int_a^b \frac{v_{at}+v_{ct}}{2} + \int_b^c v_{at}\right] \sin 3n\theta_s d\theta_s \\
&= \frac{\sqrt{3}\,V_{tm}}{2\pi}\left[\int_a^b \{\sin\theta_s + \sin(\theta_s+\frac{2\pi}{3}) \sin 3n\theta_s + \int_b^c 2 \sin\theta_s \sin 3n\theta_s\right] d\theta_s \\
&= \frac{\sqrt{6}\,V_t}{4\pi}\left[\frac{1}{1-3n}\{-\frac{1}{2}\sin(1-3n)(\frac{\pi}{6}+\alpha) + \frac{\sqrt{3}}{2}\cos(1-3n)(\frac{\pi}{6}+\alpha) - \right. \\
&\quad \frac{3}{2}\sin(1-3n)(\frac{\pi}{6}+\alpha+\mu_t) - \\
&\quad \frac{\sqrt{3}}{2}\cos(1-3n)(\frac{\pi}{6}+\alpha+\mu_t) + 2\sin(1-3n)(\frac{5\pi}{6}+\alpha)\} + \\
&\quad \frac{1}{1+3n}\{\frac{1}{2}\sin(1+3n)(\frac{\pi}{6}+\alpha) - \frac{\sqrt{3}}{2}\cos(1+3n)(\frac{\pi}{6}+\alpha) + \\
&\quad \frac{3}{2}\sin(1+3n)(\frac{\pi}{6}+\alpha+\mu_t) + \frac{\sqrt{3}}{2}\cos(1+3n)(\frac{\pi}{6}+\alpha+\mu_t) \\
&\quad \left. -2\sin(1+3n)(\frac{5\pi}{6}+\alpha)\}\right]
\end{aligned}
\tag{3.55}
$$

Therefore, the voltage $v_i(\theta_s)$ in its final form is

$$
v_i(\theta_s) = \frac{3\sqrt{2}\,V_t}{4\pi}\{\cos(\alpha+\mu_t) + \cos\alpha\} + \sum_{n=1}^{\infty}(a_n \cos n\theta_s + b_n \sin n\theta_s) \tag{3.56}
$$

Hence, the average value of voltage V_i is

$$
V_i = \frac{3\sqrt{2}\,V_t}{4\pi}\{\cos(\alpha+\mu_t) + \cos\alpha\} \tag{3.57}
$$

3.4.2 *Three-phase full-wave inverter*

The voltage and current waveforms of the three-phase full-wave inverter with a delay angle α , are shown in figure 2.12 in which the overlap angles are neglected. The conduction angle is $\frac{2\pi}{3}$. Accordingly, the current can be expressed as

$$i(\theta_s) = \frac{a_0}{2} + \sum_{n=1}^{\infty} (a_n \cos n\theta_s + b_n \sin n\theta_s) \tag{3.58}$$

where

$$a_0 = 0 \tag{3.59}$$

$$\begin{aligned} a_n &= \frac{2}{\pi} \int_{\frac{\pi}{6}+\alpha}^{\frac{5\pi}{6}+\alpha} I_{dc} \cos n\theta_s \, d\theta_s \\ &= \frac{2I_{dc}}{\pi} \frac{1}{n} [\sin n(\frac{5\pi}{6} + \alpha) - \sin n(\frac{\pi}{6} + \alpha)] \end{aligned} \tag{3.60}$$

$$\begin{aligned} b_n &= \frac{2}{\pi} \int_{\frac{\pi}{6}+\alpha}^{\frac{5\pi}{6}+\alpha} I_{dc} \sin n\theta_s \, d\theta_s \\ &= \frac{2I_{dc}}{\pi} \frac{1}{n} [-\cos n(\frac{5\pi}{6} + \alpha) + \cos n(\frac{\pi}{6} + \alpha)] \end{aligned} \tag{3.61}$$

Therefore, the inverter current $i_i(\theta_s)$ is

$$i_i(\theta_s) = \sum_{n=1}^{\infty} (a_n \cos n\theta_s + b_n \sin n\theta_s) \tag{3.62}$$

The voltage waveform has 6 pulses and has a period of $\frac{\pi}{3}$. Hence it can be written as

$$v_i(\theta_s) = \frac{a_0}{2} + \sum_{n=1}^{\infty} (a_n \cos n\theta_s + b_n \sin n\theta_s) \tag{3.63}$$

where

$$\begin{aligned} a_0 &= \frac{6}{\pi} \int_{\frac{\pi}{6}+\alpha}^{\frac{\pi}{2}+\alpha} V_{tm} \sin (\theta_s + \frac{\pi}{6})\, d\theta_s \\ &= \frac{6\sqrt{2}\, V_t}{\pi} \cos \alpha \end{aligned} \tag{3.64}$$

$$\begin{aligned} a_n &= \frac{6}{\pi} \int_{\frac{\pi}{6}+\alpha}^{\frac{\pi}{2}+\alpha} V_{tm} \sin (\theta_s + \frac{\pi}{6}) \cos 6n\,\theta_s d\theta_s \\ &= \frac{3\sqrt{2}\, V_t}{\pi} [\frac{1}{1-6n} \{ -\frac{\sqrt{3}}{2} \cos (1-6n)(\frac{\pi}{2}+\alpha) + \frac{1}{2} \sin (1-6n)(\frac{\pi}{2}+\alpha) + \\ &\quad \frac{\sqrt{3}}{2} \cos (1-6n)(\frac{\pi}{6}+\alpha) - \frac{1}{2} \sin (1-6n)(\frac{\pi}{6}+\alpha)\} \\ &\quad \frac{1}{1+6n} \{ -\frac{\sqrt{3}}{2} \cos(1+6n)(\frac{\pi}{2}+\alpha) + \frac{1}{2} \sin (1+6n)(\frac{\pi}{2}+\alpha) \\ &\quad \frac{\sqrt{3}}{2} \cos (1+6n)(\frac{\pi}{6}+\alpha) + \frac{1}{2} \sin (1+6n)(\frac{\pi}{6}+\alpha)\}] \end{aligned} \tag{3.65}$$

$$b_n = \frac{6}{\pi}\int_{\frac{\pi}{6}+\alpha}^{\frac{\pi}{2}+\alpha} V_{tm} \sin\ (\theta_s + \frac{\pi}{6})\ \sin\ 6n\theta_s\, d\theta_s$$

$$= \frac{3\sqrt{2}\,V_t}{\pi}[\frac{1}{1-6n}\{\frac{\sqrt{3}}{2}\ \sin\ (1-6n)(\frac{\pi}{2}+\alpha) + \frac{1}{2}\cos\ (1-6n)(\frac{\pi}{2}+\alpha) -$$

$$\frac{\sqrt{3}}{2}\ \cos\ (1-6n)(\frac{\pi}{6}+\alpha) - \frac{1}{2}\ \sin\ (1-6n)(\frac{\pi}{6}+\alpha)\} \qquad (3.66)$$

$$\frac{1}{1+6n}\{-\frac{\sqrt{3}}{2}\ \sin(1+6n)(\frac{\pi}{2}+\alpha) - \frac{1}{2}\cos\ (1+6n)(\frac{\pi}{2}+\alpha)$$

$$\frac{\sqrt{3}}{2}\ \sin\ (1+6n)(\frac{\pi}{6}+\alpha) + \frac{1}{2}\ \cos\ (1+6n)(\frac{\pi}{6}+\alpha)\}]$$

Therefore, the voltage $v_i(\theta_s)$ is expressed in its final form as

$$v_i(\theta_s) = \frac{3\sqrt{2}\,V_t}{\pi}\ \cos\ \alpha + \sum_{n=1}^{\infty}(a_n\ \cos\ 6n\,\theta_s + b_n\ \sin\ 6n\,\theta_s) \qquad (3.67)$$

The waveforms of the voltage and current in a three-phase full-wave inversion mode with an overlap angle μ_t are shown in figure 2.14.

As shown in figure 2.13 (b) the current waveform has a period of 2π. It can be written as

$$i(\theta_s) = \frac{a_0}{2} + \sum_{n=1}^{\infty}(\,a_n\ \cos\ n\theta_s + b_n\ \sin\ n\theta_s) \qquad (3.68)$$

where

$$a_0 = 0 \qquad (3.69)$$

$$a_n = \frac{1}{\pi}\left[\int_a^b \frac{I_{dc}}{\mu_t}(\theta_s - a) + \int_b^c I_{dc} - \int_c^d \frac{I_{dc}}{\mu_t}(\theta_s - d) + \right.$$
$$\left.\int_e^f \frac{I_{dc}}{\mu_t}(\theta_s - e) - \int_f^g I_{dc} - \int_g^h \frac{I_{dc}}{\mu_t}(\theta_s - h)\right] \cos\ n\theta_s\, d\theta_s$$
$$= \frac{I_{dc}}{\pi}\frac{1}{n^2\mu_t}(\cos\ nb - \cos\ na - \cos\ nd + \cos\ nc + \cos\ nf - \cos\ ne - \cos\ nh + \cos\ ng) \tag{3.70}$$
$$= \frac{I_{dc}}{\pi}\frac{1}{n^2\mu_t}\{\cos\ n(\frac{\pi}{6} + \alpha + \mu) - \cos\ n(\frac{\pi}{6} + \alpha) - \cos\ n(\frac{5\pi}{6} + \alpha + \mu_t) +$$
$$\cos(\frac{5\pi}{6} + \alpha) - \cos\ n(\frac{7\pi}{6} + \alpha + \mu_t) + \cos\ n(\frac{7\pi}{6} + \alpha) -$$
$$\cos\ n(\frac{11\pi}{6} + \alpha + \mu_t) + \cos\ n(\frac{11\pi}{6} + \alpha)\}$$

$$b_n = \frac{1}{\pi}\left[\int_a^b \frac{I_{dc}}{\mu_t}(\theta_s - a) + \int_b^c I_{dc} - \int_c^d \frac{I_{dc}}{\mu_t}(\theta_s - d) + \right.$$
$$\left.\int_e^f \frac{I_{dc}}{\mu_t}(\theta_s - e) - \int_f^g I_{dc} - \int_g^h \frac{I_{dc}}{\mu_t}(\theta_s - h)\right] \cos\ n\theta_s\, d\theta_s$$
$$= \frac{I_{dc}}{\pi}\frac{1}{n^2\mu_t}(\sin\ nb - \sin\ na - \sin\ nd + \sin\ nc + \sin\ nf - \sin\ ne - \sin\ nh + \sin\ ng) \tag{3.71}$$
$$= \frac{I_{dc}}{\pi}\frac{1}{n^2\mu_t}\{\sin\ n(\frac{\pi}{6} + \alpha + \mu) - \sin\ n(\frac{\pi}{6} + \alpha) - \sin\ n(\frac{5\pi}{6} + \alpha + \mu_t) +$$
$$\sin(\frac{5\pi}{6} + \alpha) - \sin\ n(\frac{7\pi}{6} + \alpha + \mu_t) + \sin\ n(\frac{7\pi}{6} + \alpha) +$$
$$\sin\ n(\frac{11\pi}{6} + \alpha + \mu_t) - \sin\ n(\frac{11\pi}{6} + \alpha)\}$$

Threrfore the current $i_i(\theta_s)$ is

$$i_i(\theta_s) = \sum_{n=1}^{\infty}(a_n \cos\ n\theta_s + b_n \sin\ n\theta_s) \tag{3.72}$$

Since the voltage waveform has a period of $\frac{2\pi}{3}$, the voltage can be expressed as

$$v_i(\theta_s) = \frac{a_0}{2} + \sum_{n=1}^{\infty} (a_n \cos n\theta_s + b_n \sin n\theta_s) \tag{3.73}$$

where

$$\begin{aligned} a_0 = \frac{6}{\pi} [& \int_{\frac{\pi}{6}+\alpha}^{\frac{\pi}{6}+\alpha+\mu_t} \frac{V_{tm}}{2} \{ \sin(\theta_s + \frac{\pi}{6}) + \sin(\theta_s + \frac{\pi}{2}) + \\ & \int_{\frac{\pi}{6}+\alpha+\mu_t}^{\frac{\pi}{2}+\alpha} V_{tm} \sin(\theta_s + \frac{\pi}{6})] \, d\theta_s \\ = & \frac{3\sqrt{2}\, v_t}{2\pi} \{ \cos \alpha + \cos (\alpha + \mu_t) \} \end{aligned} \tag{3.74}$$

$$\begin{aligned} a_n = & \frac{6}{\pi} [\int_{\frac{\pi}{6}+\alpha}^{\frac{\pi}{6}+\alpha+\mu_t} \frac{V_{tm}}{2} \{ \sin(\theta_s + \frac{\pi}{6}) + \sin(\theta_s + \frac{\pi}{2}) \} + \\ & \int_{\frac{\pi}{6}+\alpha+\mu_t}^{\frac{\pi}{2}+\alpha} V_{tm} \sin(\theta_s + \frac{\pi}{6})] \cos 6n\theta_s \, d\theta_s \\ = & \frac{3V_{tm}}{2\pi} [\frac{1}{1-6n} \{ \frac{1}{2} \sin(1-6n)(\frac{\pi}{6} + \mu_t) + \frac{\sqrt{3}}{2} \cos(1-6n)(\frac{\pi}{6} + \alpha) - \\ & \frac{3}{2} \sin(1-6n)(\frac{\pi}{6} + \alpha) - \sqrt{3} \cos(1-6n)(\frac{\pi}{2} + \alpha) + \\ & \sin(1-6n)(\frac{\pi}{2} + \alpha) + \frac{\sqrt{3}}{2} \cos(1-6n)(\frac{\pi}{6} + \alpha + \mu_t) \} + \\ & \frac{1}{1+6n} \{ \frac{1}{2} \sin(1+6n)(\frac{\pi}{6} + \mu_t) + \frac{\sqrt{3}}{2} \cos(1+6n)(\frac{\pi}{6} + \alpha) - \\ & \frac{3}{2} \sin(1+6n)(\frac{\pi}{6} + \alpha) - \sqrt{3} \cos(1+6n)(\frac{\pi}{2} + \alpha) + \\ & \sin(1+6n)(\frac{\pi}{2} + \alpha) + \frac{\sqrt{3}}{2} \cos(1+6n)(\frac{\pi}{6} + \alpha + \mu_t) \}] \end{aligned} \tag{3.75}$$

$$b_n = \frac{6}{\pi}[\int_{\frac{\pi}{6}+\alpha}^{\frac{\pi}{6}+\alpha+\mu_t} \frac{V_{tm}}{2}\{\sin(\theta_s+\frac{\pi}{6})+\sin(\theta_s+\frac{\pi}{2})\}+$$

$$\int_{\frac{\pi}{6}+\alpha+\mu_t}^{\frac{\pi}{2}+\alpha} V_{tm}\sin(\theta_s+\frac{\pi}{6})]\sin 6n\theta_s\, d\theta_s$$

$$= \frac{3V_{tm}}{2\pi}[\frac{1}{1-6n}\{\frac{1}{2}\cos(1-6n)(\frac{\pi}{6}+\mu_t)-\frac{\sqrt{3}}{2}\sin(1-6n)(\frac{\pi}{6}+\alpha)-$$

$$\frac{3}{2}\sin(1-6n)(\frac{\pi}{6}+\alpha)+\sqrt{3}\sin(1-6n)(\frac{\pi}{2}+\alpha)- \qquad (3.76)$$

$$\cos(1-6n)(\frac{\pi}{2}+\alpha)-\frac{\sqrt{3}}{2}\sin(1-6n)(\frac{\pi}{6}+\alpha+\mu_t)\}+$$

$$\frac{1}{1+6n}\{-\frac{1}{2}\cos(1+6n)(\frac{\pi}{6}+\mu_t)+\frac{\sqrt{3}}{2}\sin(1+6n)(\frac{\pi}{6}+\alpha)+$$

$$\frac{3}{2}\sin(1+6n)(\frac{\pi}{6}+\alpha)-\sqrt{3}\sin(1+6n)(\frac{\pi}{2}+\alpha)+$$

$$-\cos(1+6n)(\frac{\pi}{2}+\alpha)+\frac{\sqrt{3}}{2}\sin(1+6n)(\frac{\pi}{6}+\alpha+\mu_t)\}]$$

Therefore, the voltage $v_i(\theta_s)$ is

$$v_i(\theta_s) = \frac{3\sqrt{2}\,V_t}{2\pi}\{\cos\alpha+\cos(\alpha+\mu_t)\}+\sum_{n=1}^{\infty}(a_n\cos 6n\,\theta_s+b_n\sin 6n\,\theta_s) \qquad (3.77)$$

Hence, the average value of voltage V_i is

$$V_i = \frac{3\sqrt{2}\,V_t}{2\pi}\{\cos\alpha+\cos(\alpha+\mu_t)\} \qquad (3.78)$$

Figures 3.1, 3.2, 3.3 and 3.4 show the magnitudes of the voltage harmonics of a 6 pulse phase-controlled converter with respect to the triggering angle with some overlap-angles.

The figures show that the triggering angle and the overlap angle influence the magnitudes of the voltage harmonics. Compared to the voltage harmonics, the magnitudes of the current harmonics are independent of the triggering angle as shown in equation (3.40).

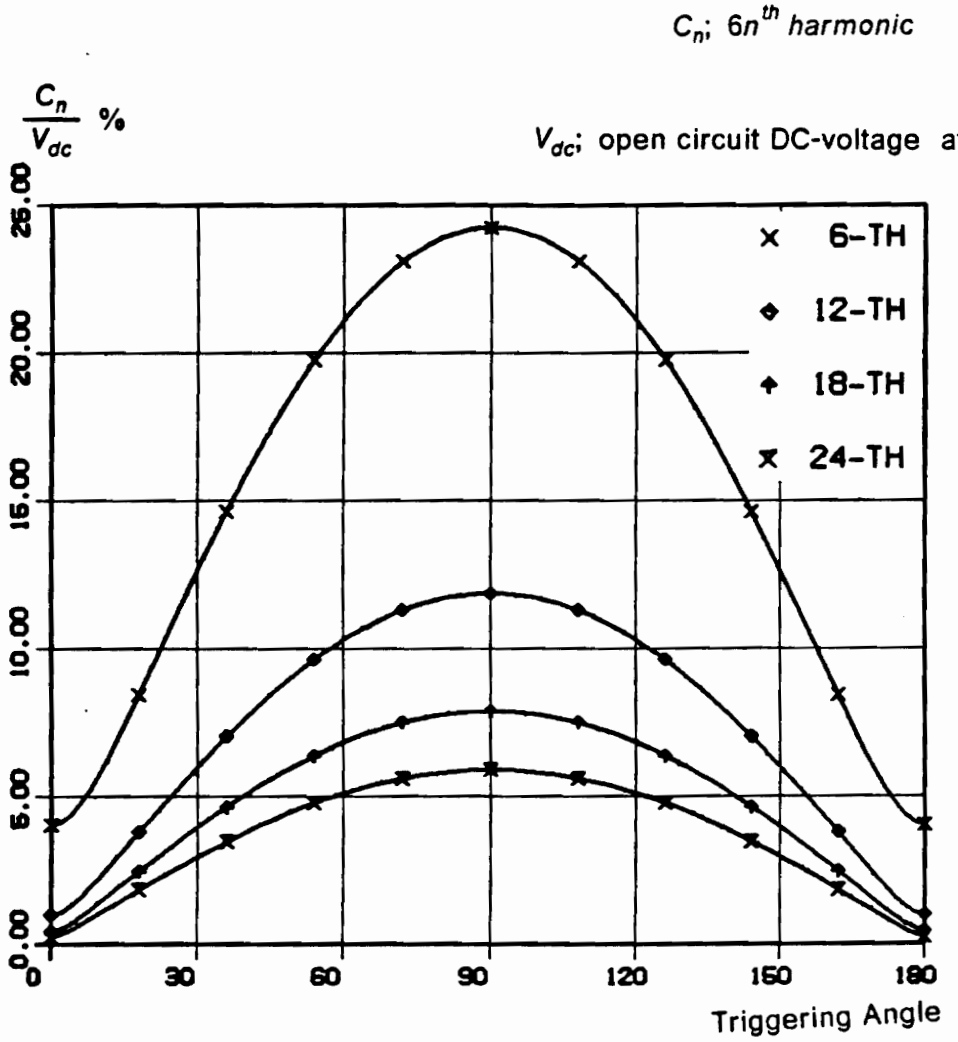

Figure 3.1 Triggering angle vs harmonics' magnitude (overlap = 0. deg)

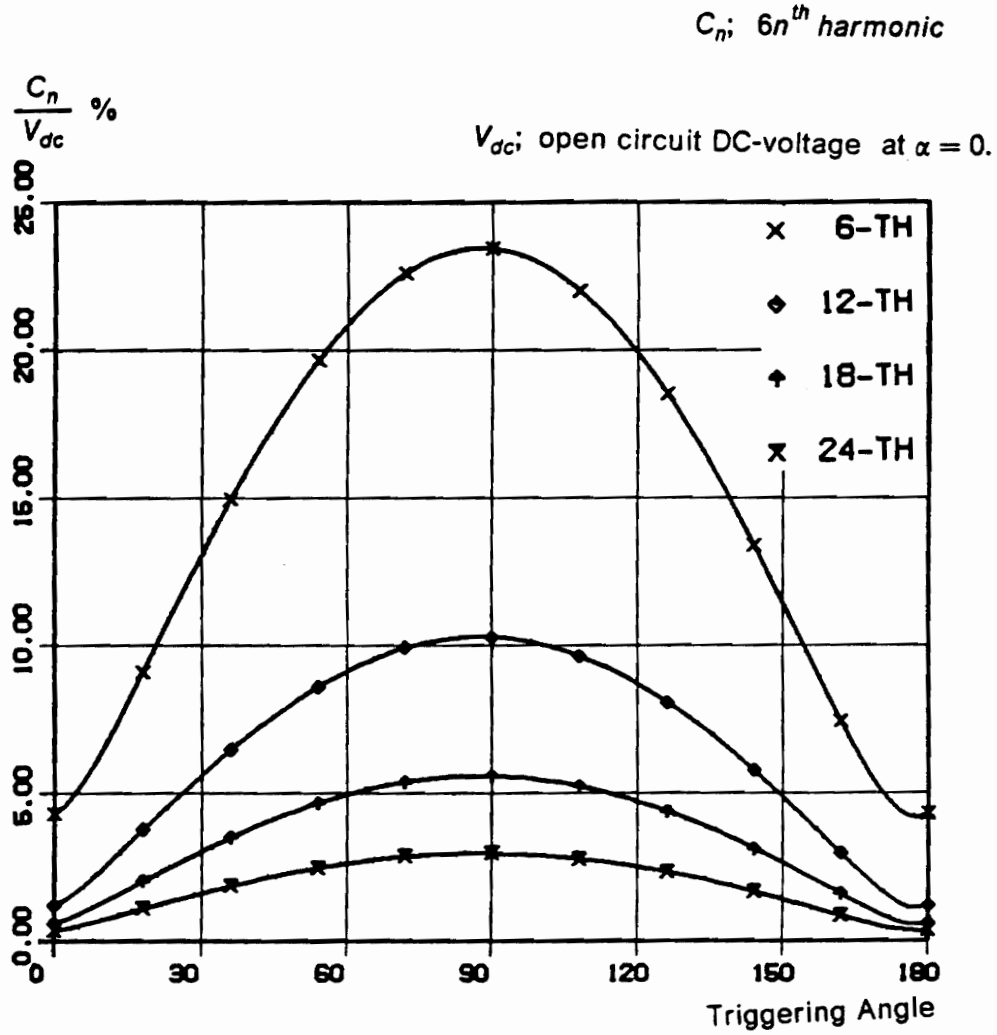

Figure 3.2 Triggering angle vs harmonics' magnitude (overlap = 5. deg)

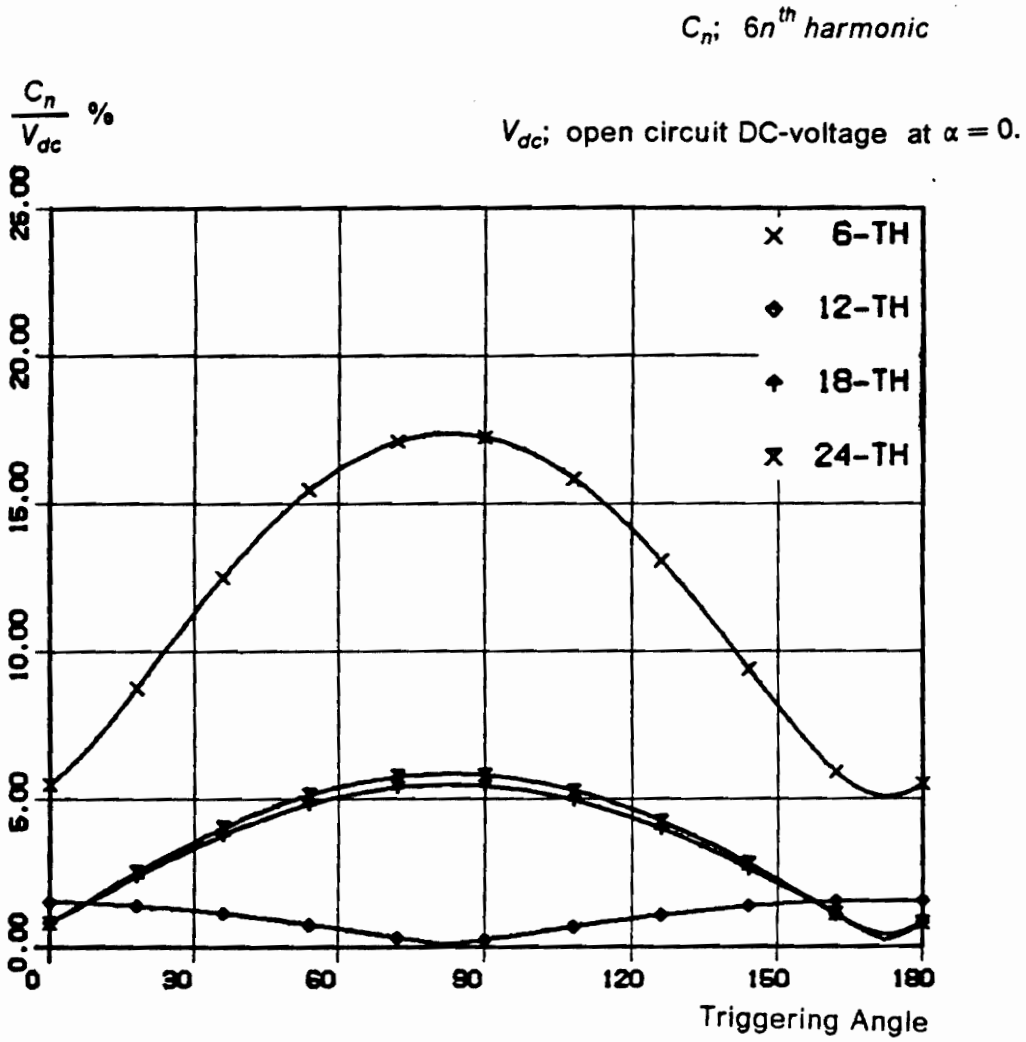

Figure 3.3 Triggering angle vs harmonics' magnitude (overlap = 15. deg)

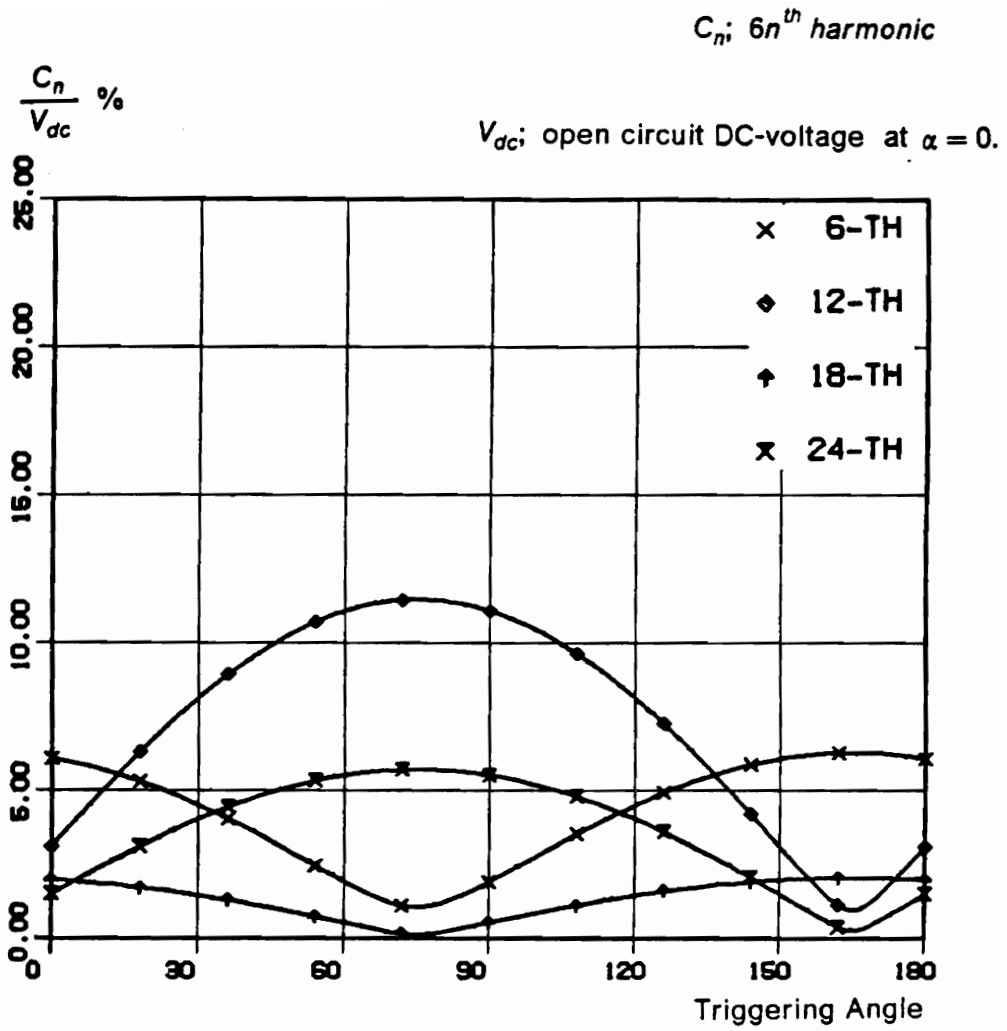

Figure 3.4 Triggering angle vs harmonics' magnitude (overlap = 30. deg)

Chapter 4. Experimental correlation of VSCF power conversion scheme with PMSG-Half wave inverter case

4.1 Introduction

This section consists of the experimental correlation of the performance prediction of the VSCF power conversion scheme with PMSG. Only half-wave inverter case is considered for comparison. The experimental set-up is described and salient performance characteristics are obtained.

4.2 Experimental set-up

The experimental set-up with half-wave inverter is shown in figure 4.1. The variable speed prime mover is a permanent magnet dc brush motor. Its speed is varied by controlling the ac input voltages to the bridge rectifier with an auto transformer.

The output voltages of the PMSG are rectified and fed to a dc link filter which in turn is connected to the half-wave phase controlled converter. The input to the converter from its ac side is through a three phase transformer.

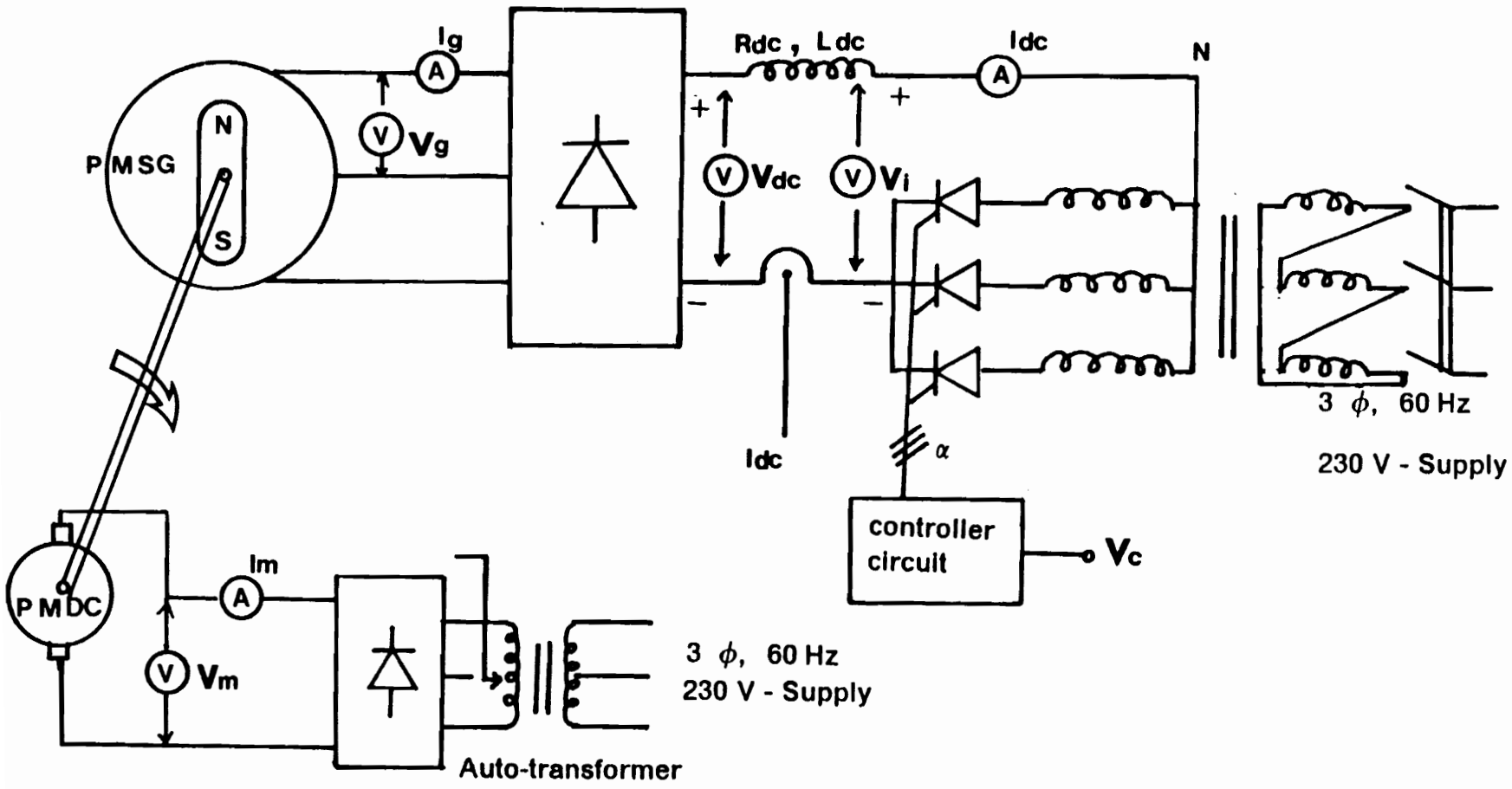

Figure 4.1 Experimental set-up of VSCF power conversion scheme with the half-wave inverter

An analog control circuit has been designed and built to convert the control signal v_c to an equivalent triggering angle α . This control circuit is shown in figure 4.2. Even though the triggering angle can be changed from 0°to180° , this application requires the operation from 90°to155° . The upper limit of 155° is to give sufficient time for the SCRs to turn-off and recover their forward blocking capability.

4.3 Experimental results

The predicted and experimental rectified voltage of the PMSG is shown in figure 4.3. The details of the PMSG is given in Appendix-1. The generator is driven at 757 rpm and has an overlap angle of 19° . The close correlation between the predicted and experimental waveforms and their magnitudes is evident from figure 4.3. The slight dissimilarity in the rectified voltage is due to the asymmetry of the induced emfs in the phasewindings of the PMSG. The output dc voltage of the controlled converter is shown in figure 4.4. The predicted and experimental waveforms are practically identical. This corresponds to a triggering angle of 127° .

The SCR current and phase voltage is shown in figure 4.5. The dc link current, I_{dc} and the dc voltage of the inverter, V_i are shown in figure 4.6. Note that the dc link current has a high ripple current as the dc link filter is not sufficient to filter the 3^{rd} harmonic generated by the inverter and the 6^{th} harmonic generated from the PMSG side rectification.

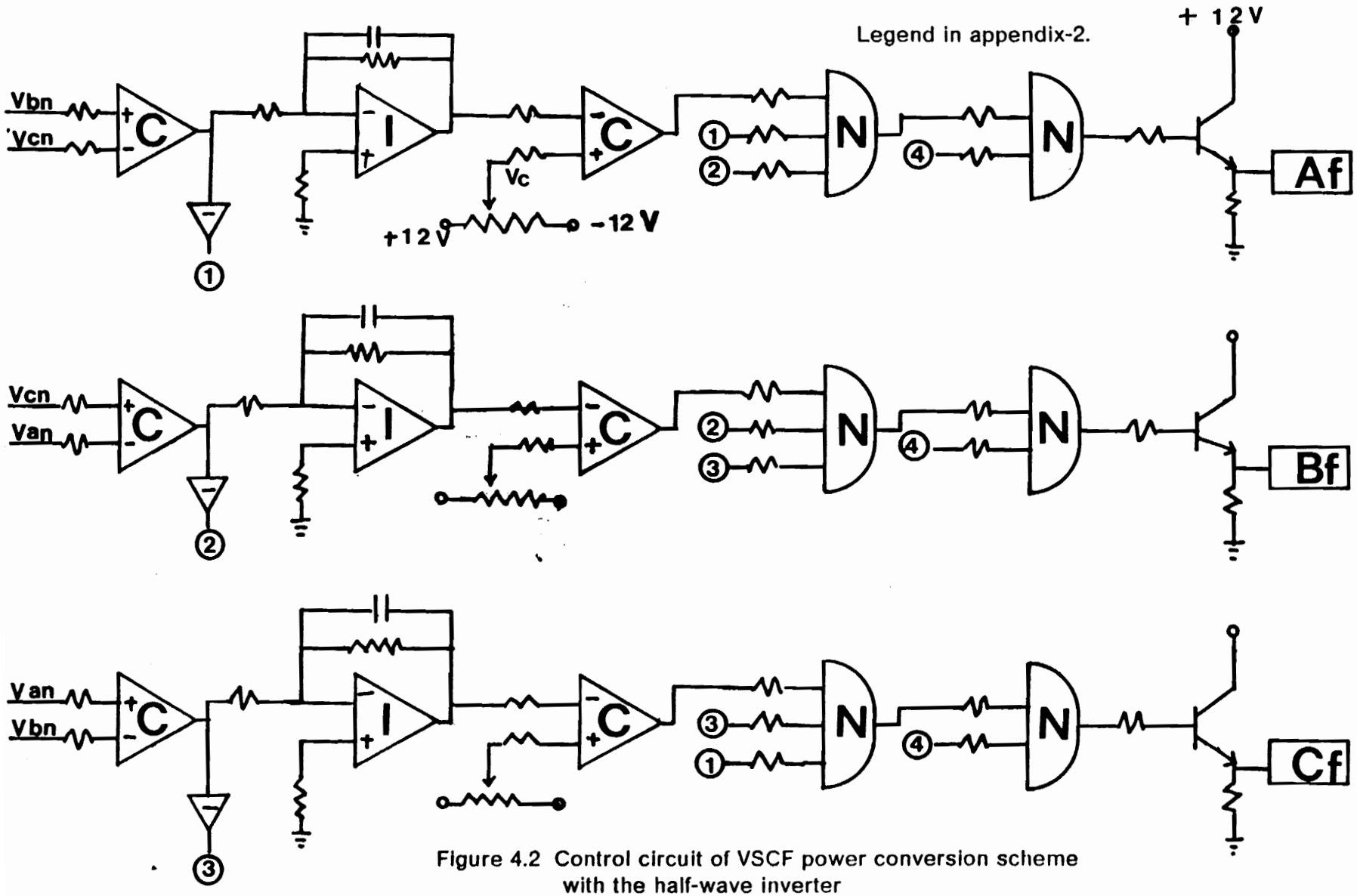

Figure 4.2 Control circuit of VSCF power conversion scheme with the half-wave inverter
(a) Analog control circuit

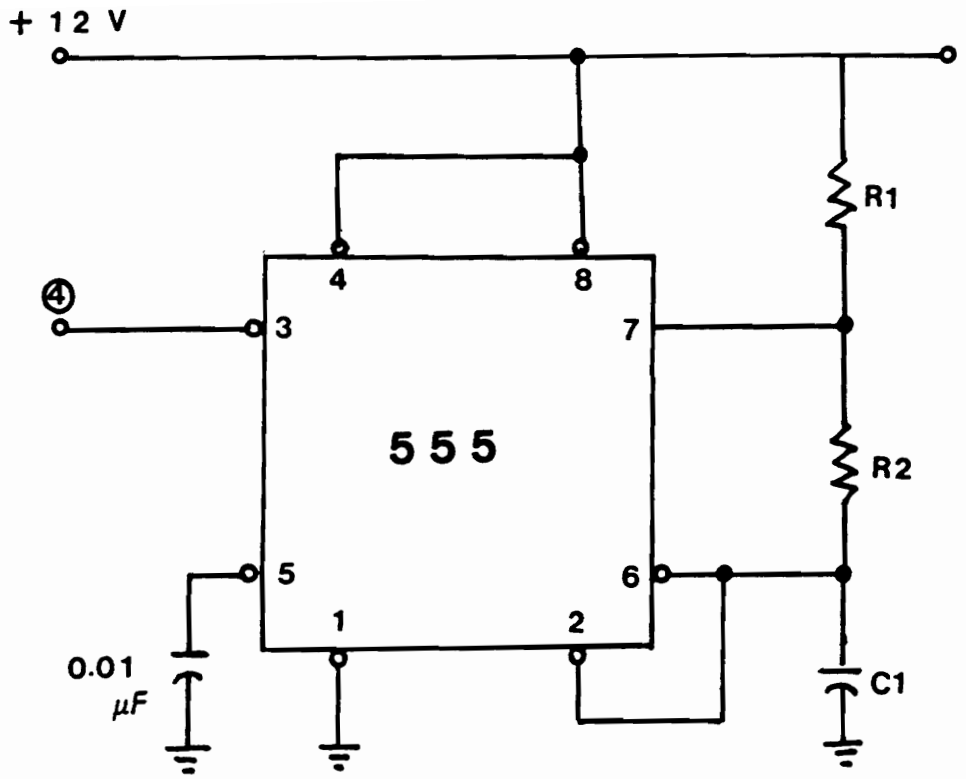

$$f = \frac{1.44}{(R_1 + 2R_2)C_1} \text{ (Frequency)}$$

$$D = \frac{R_2}{R_1 + 2R_2} \text{ (Duty cycle)}$$

Figure 4.2 Control circuit of VSCF power conversion scheme with the half-wave inverter
(b) Pulse generator circuit

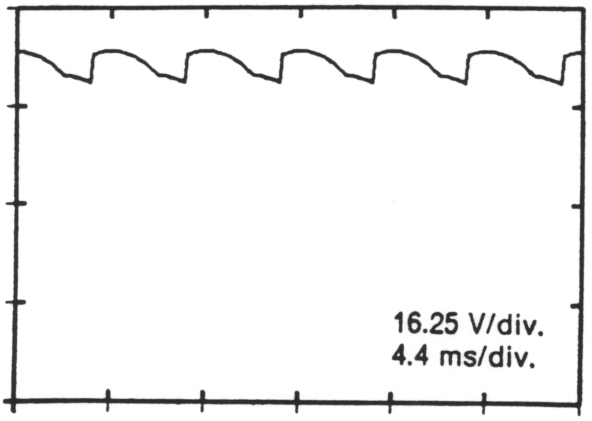

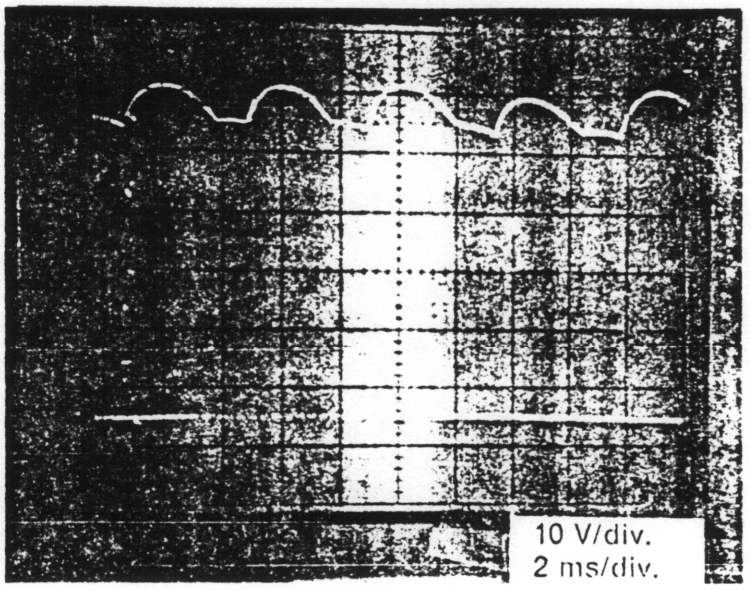

Figure 4.3 The predicted and experimental waveforms of the rectified PMSG voltage (757 rpm, overlap = 19 deg., 4A, Resistive load)

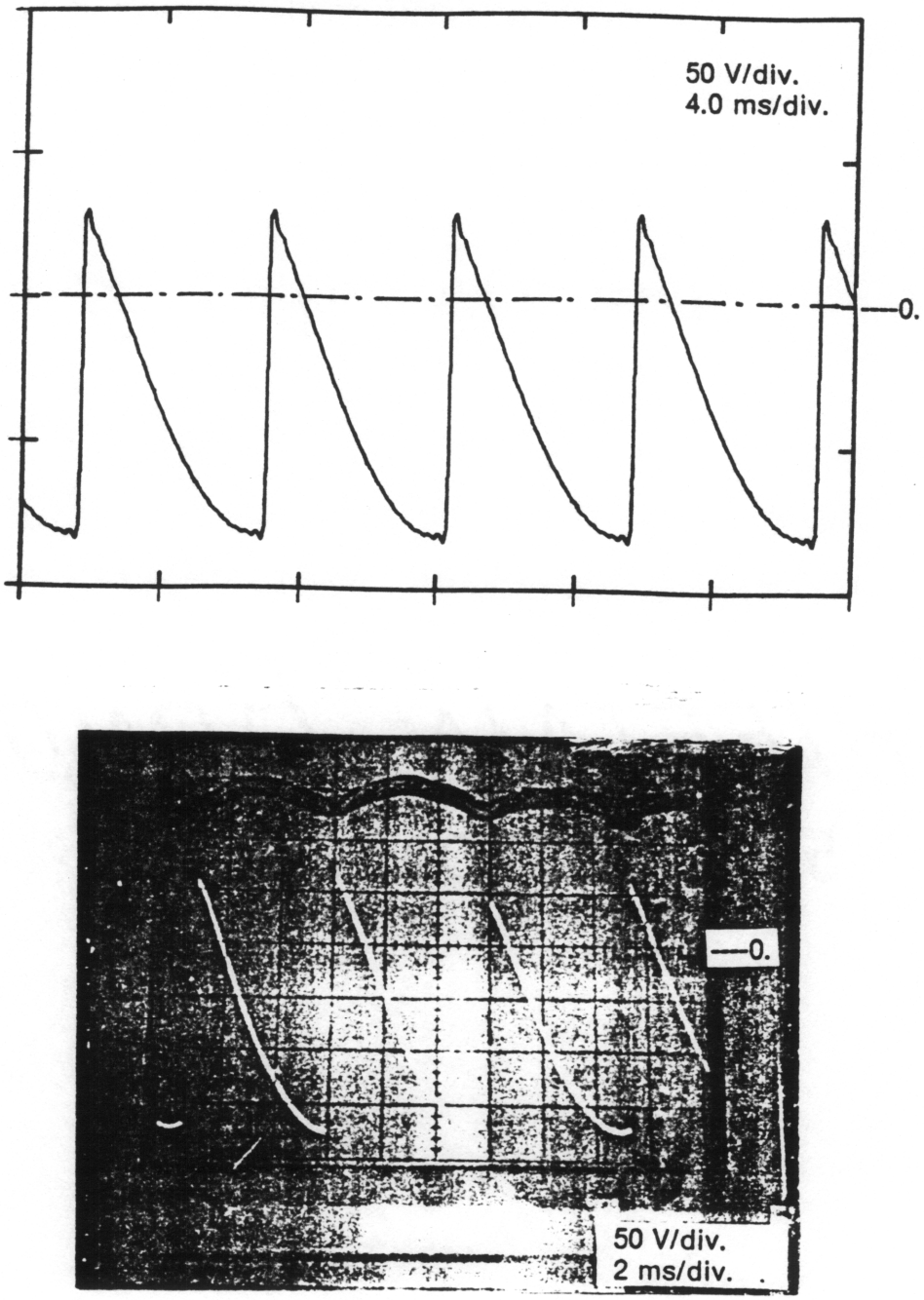

Figure 4.4 The predicted and experimental inverted output voltage waveforms of the THWI at $\alpha = 127°$, N = 1280 rpm

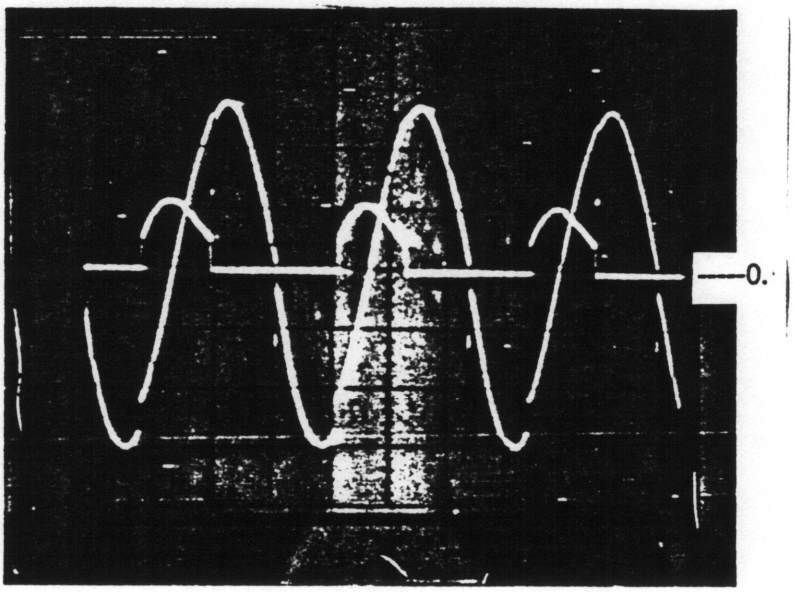

Figure 4.5 The current in the SCR and phase voltage of the supply at $\alpha = 127°$, N = 1280 rpm (100 V/div., 5 ms/div.)

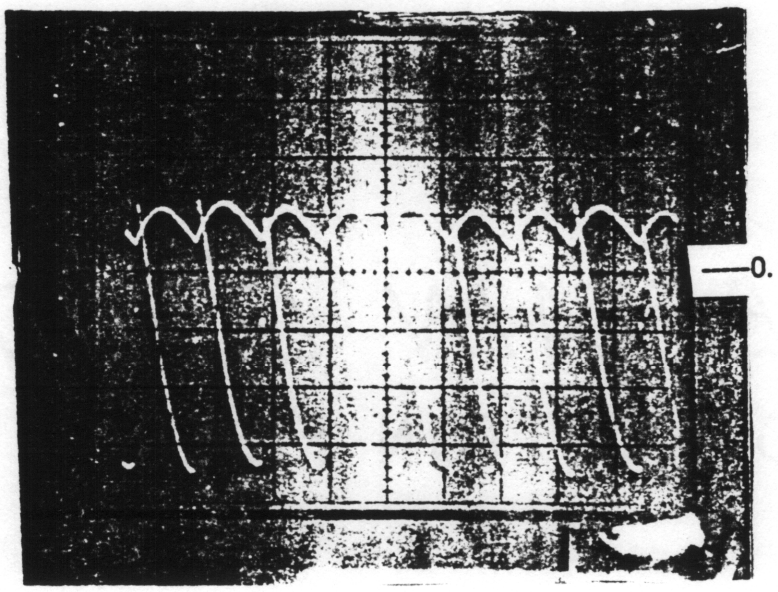

Figure 4.6 The waveforms of I_{dc} and V_l for THWI at $\alpha = 124°$, N = 1280 rpm
(5 A/div. 50 V/div. 5 ms/div)

4.4 Comparison of performance characteristics

Triggering angle, α vs speed of the PMSG at 100 % and 75 % of rated dc link current are shown in figures 4.7 and 4.8, respectively. There is a close correlation between the theoretical and experimental results. Figures 4.9 and 4.10 show the active power vs speed of the PMSG at 100 % and 75 % of rated dc link currents, respectively. This power corresponds to the power sent to the constant frequency ac supply. The prediction is extremely close to the experimental values as shown. Such close correlation is also seen in the reactive power, drawn from the constant frequency ac supply, as shown in figures 4.11 and 4.12 for 100 % and 75 % of rated dc link current, respectively. The correlation of the power factor is shown in figures 4.13 and 4.14.

The overall efficiency is defined as the ratio of the power transferred to the ac constant frequency supply to the output of air gap power of the PMSG. The overall efficiency vs speed for 100 % and 75 % of rated dc link currents are shown in figures 4.15 and 4.16, respectively. The discrepancy between the predicted and measured results is due to the difficulty of accounting for losses in the power devices. It is also compounded by the fact that harmonic losses have not been rigorously considered in this thesis. The high efficiencies at part load and at low speeds are in favor of the VSCF power conversion scheme as is seen from the simulation and experimental results.

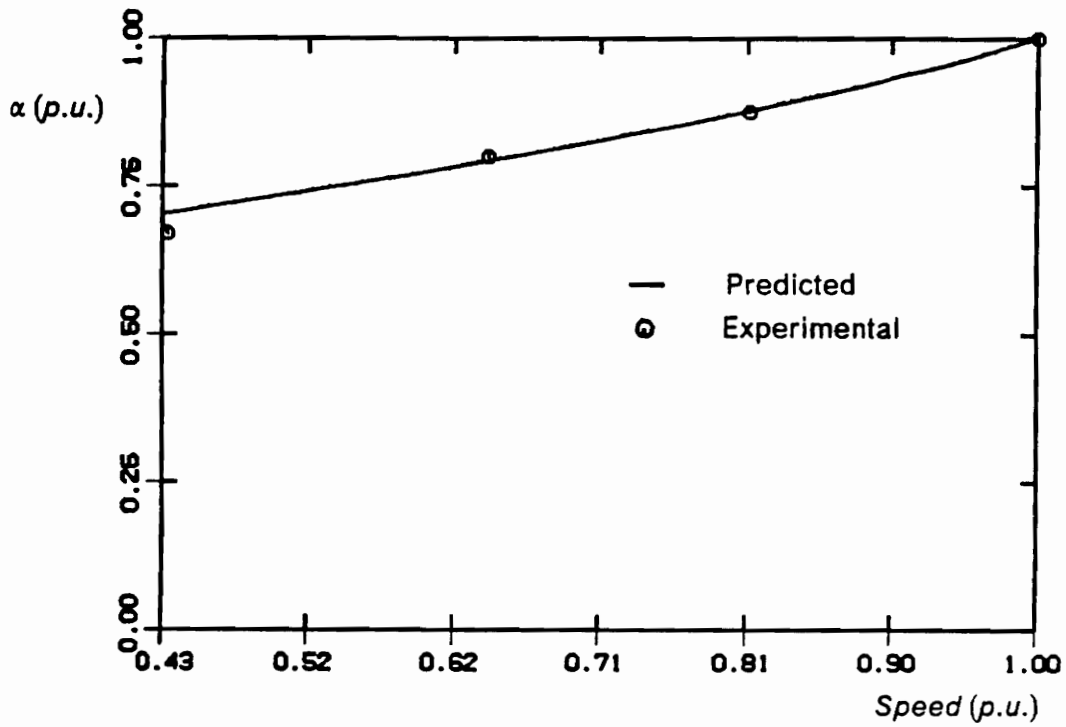

Figure 4.7 Triggering angle vs speed characteristics at 100 % I_{dc}

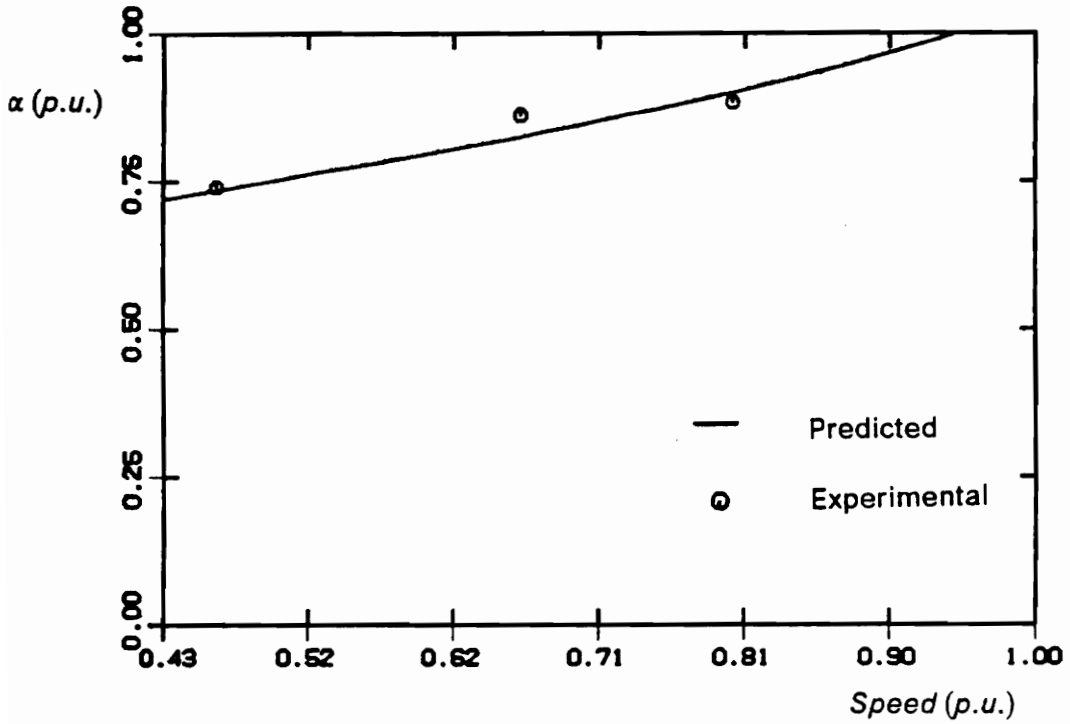

Figure 4.8 Triggering angle vs speed characteristics at 75 % I_{dc}

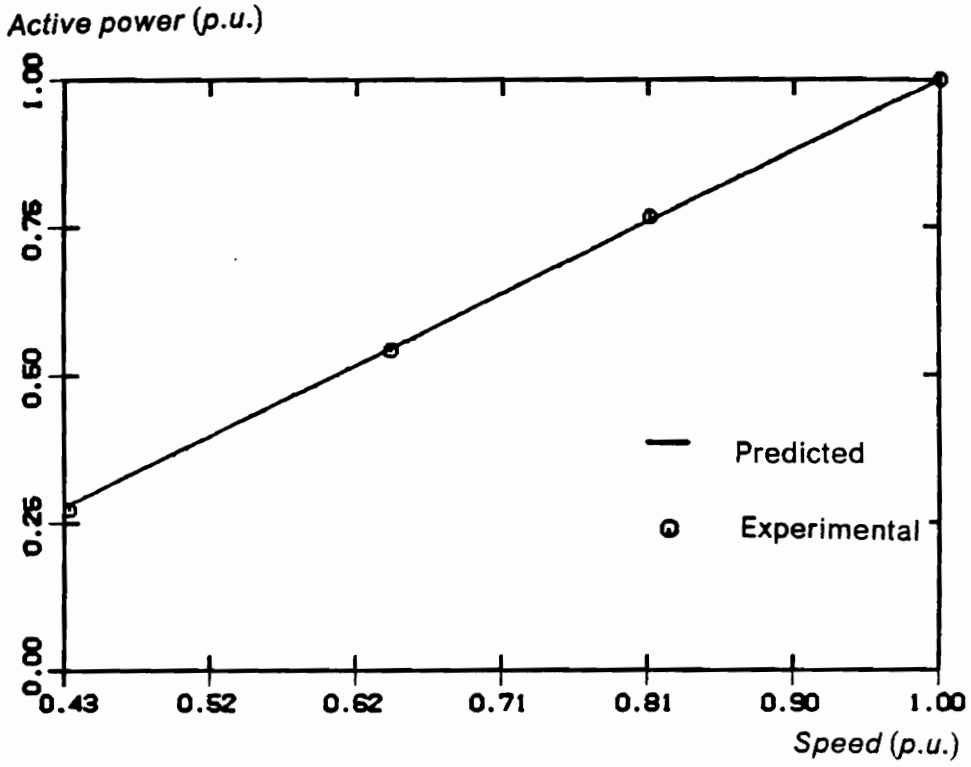

Figure 4.9 Active power vs speed characteristics at 100 % I_{dc}

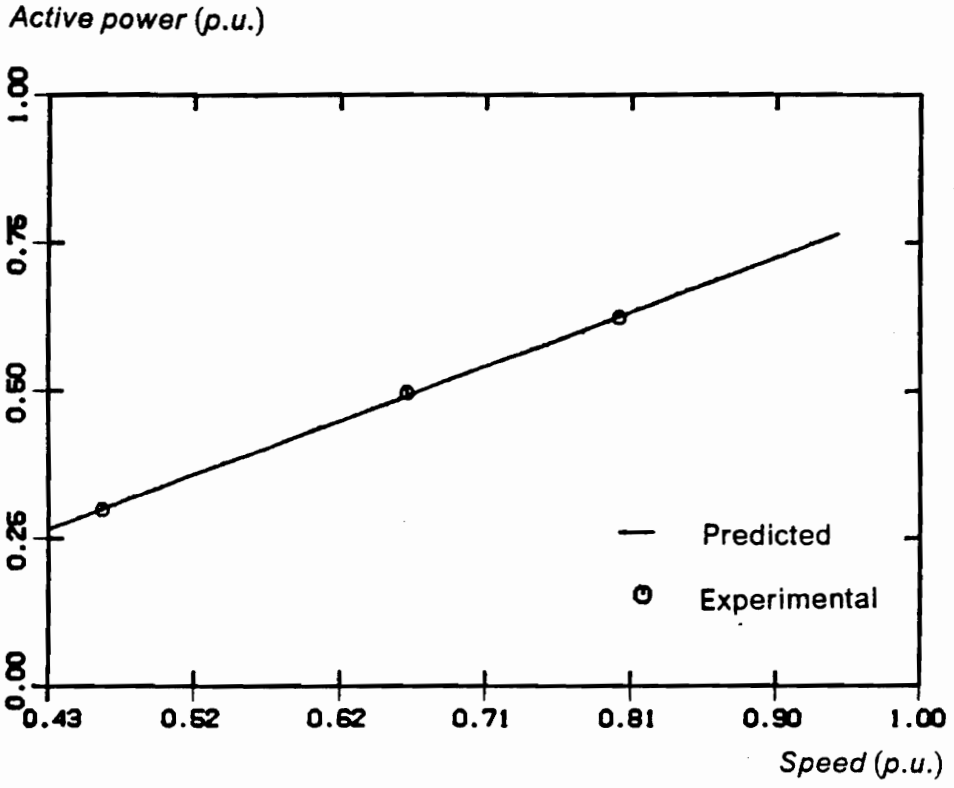

Figure 4.10 Active power vs speed characteristics at 75 % I_{dc}

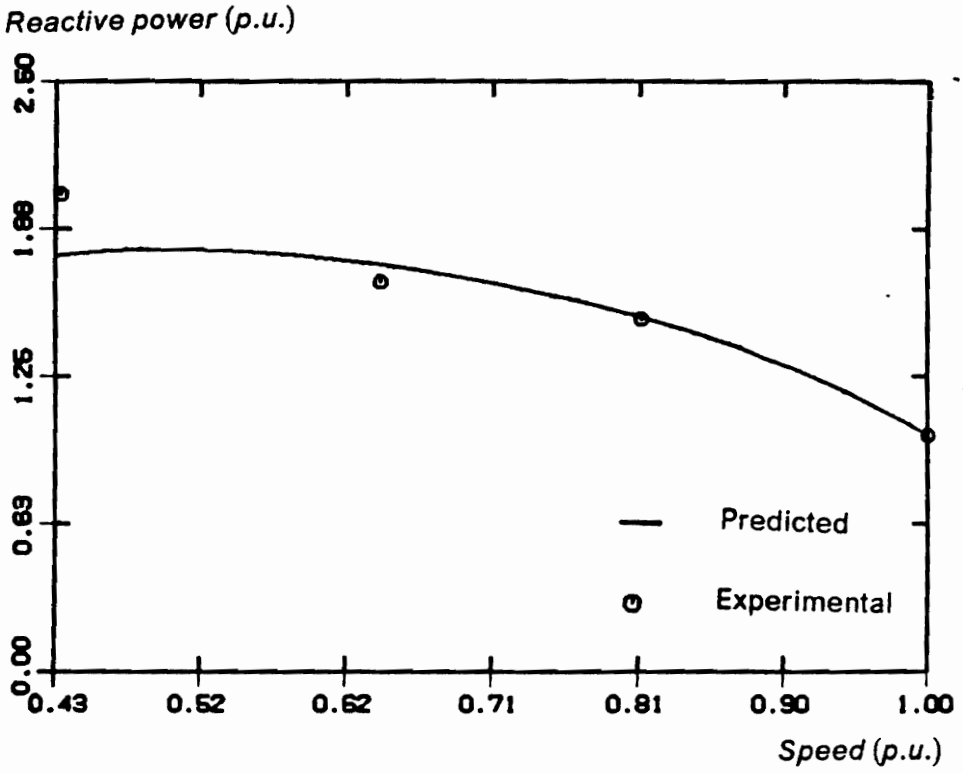

Figure 4.11 Reactive power vs speed characteristics at 100 % I_{dc}

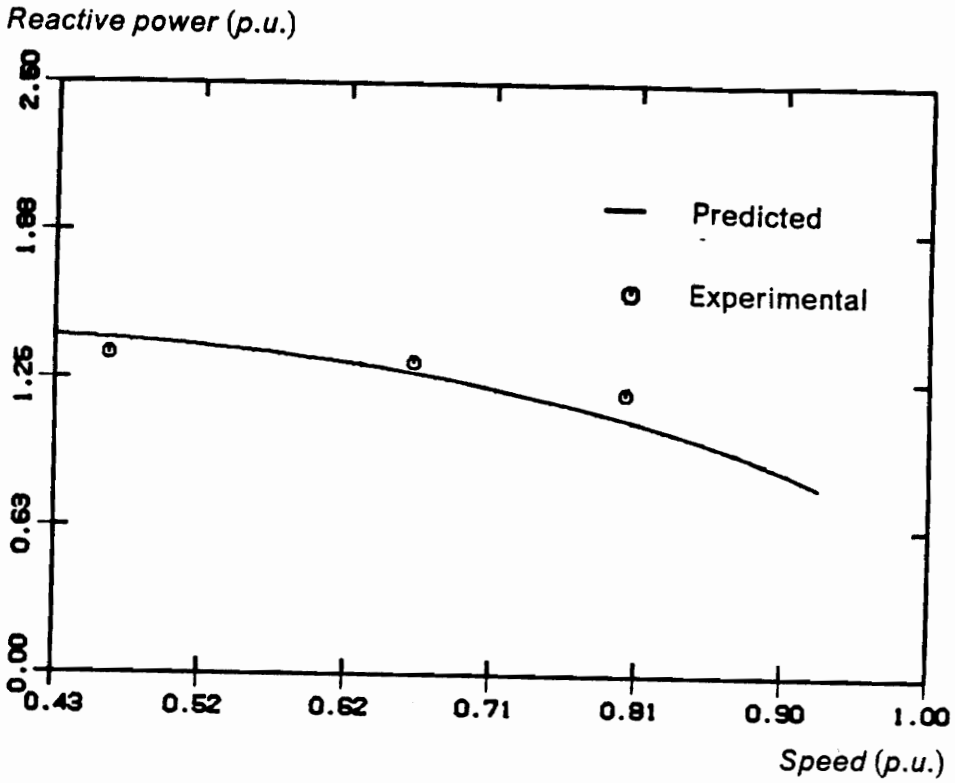

Figure 4.12 Reactive power vs speed characteristics at 75 % I_{dc}

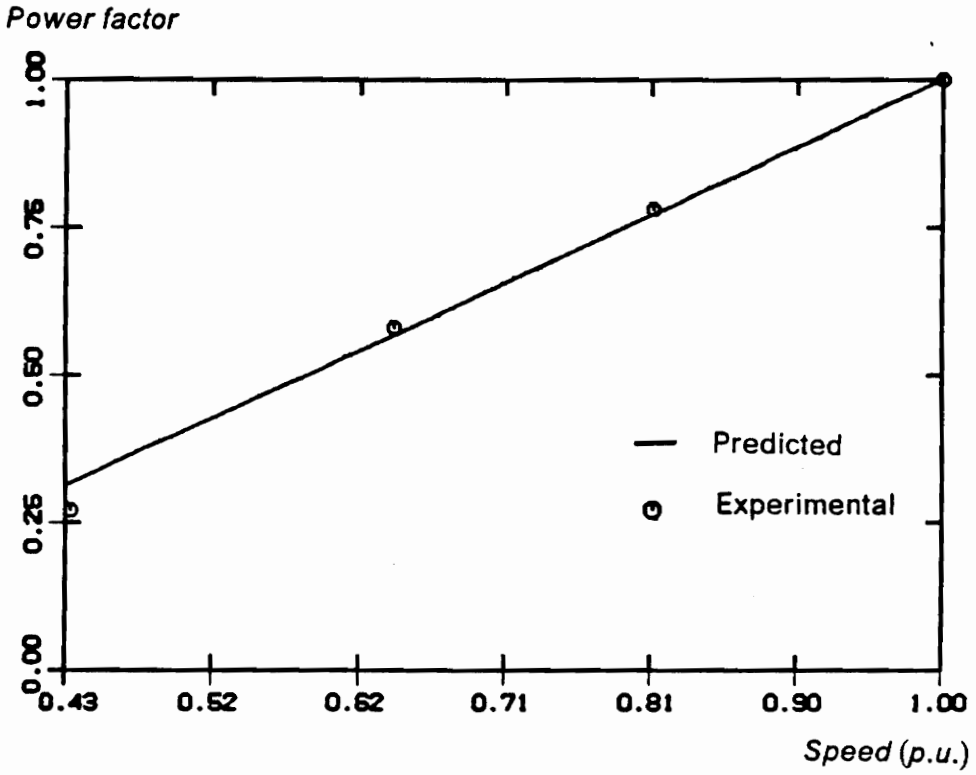

Figure 4.13 Power factor vs speed characteristics at 100 % I_{dc}

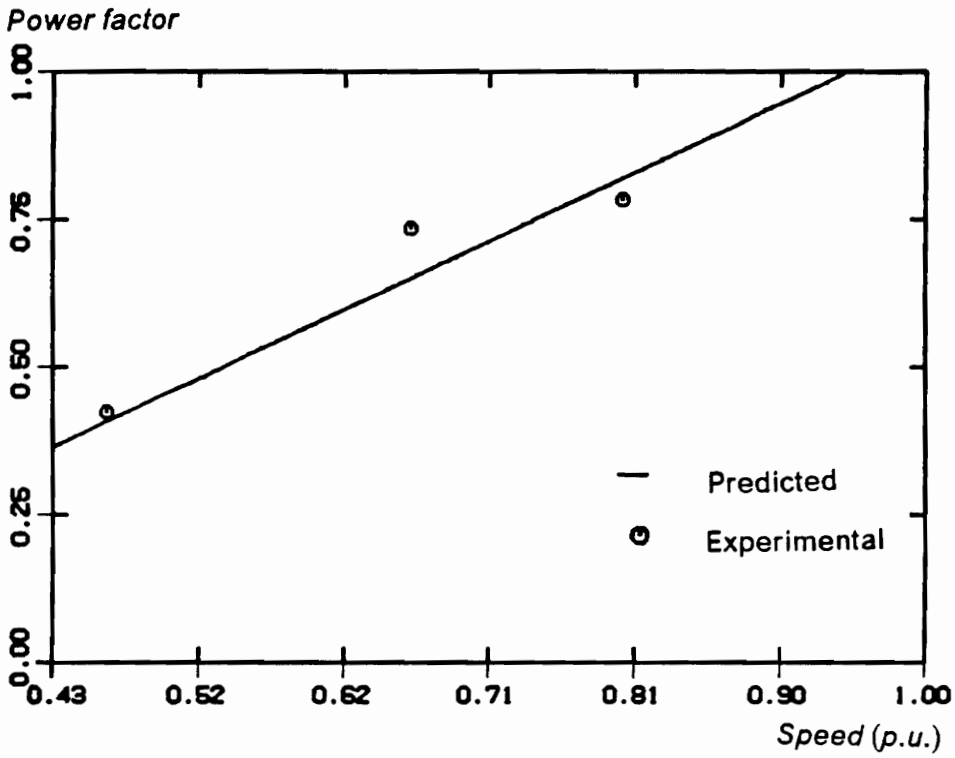

Figure 4.14 Power factor vs speed characteristics at 75 % I_{dc}

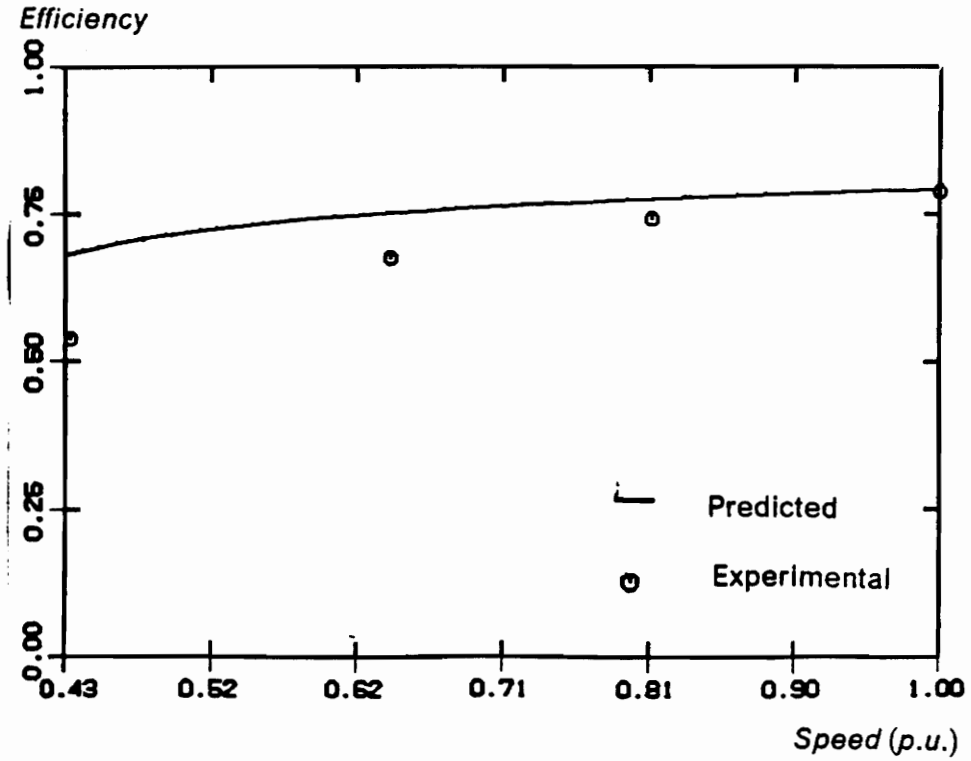

Figure 4.15 Overall efficiency vs speed characteristics at 100 % I_{dc}

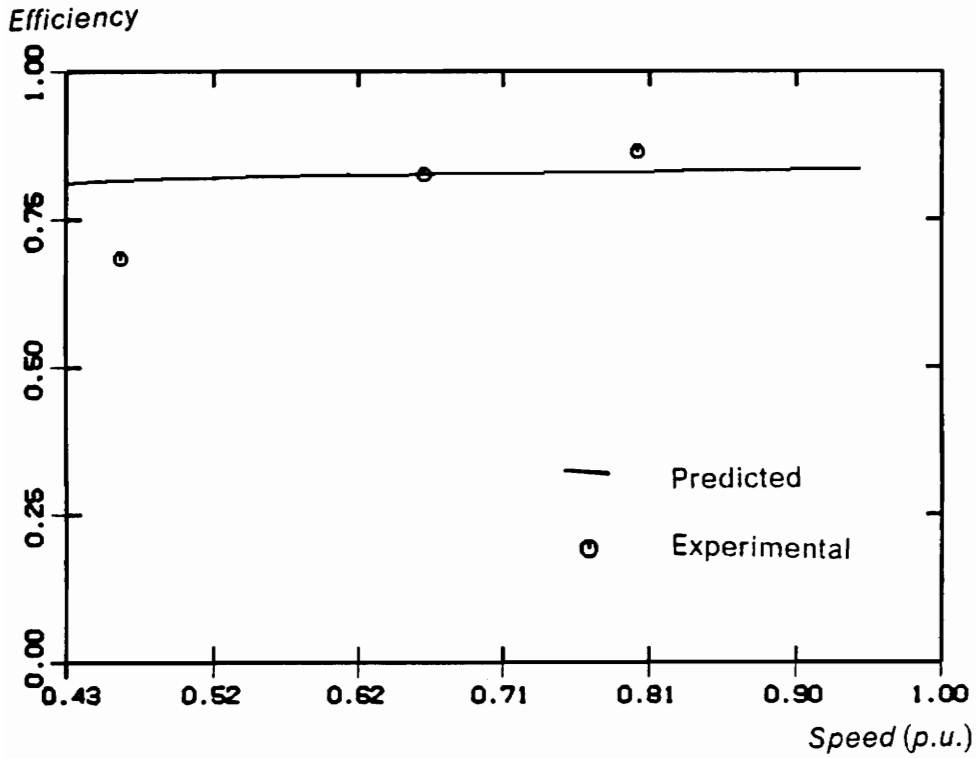

Figure 4.16 Overall efficiency vs speed characteristics at 75 % I_{dc}

5. CONCLUSION

5.1 Introduction

This chapter contains the conclusions on the study of VSCF power conversion scheme with PMSG related to its steady state operation. Recommendations for future study on this topic are made.

5.2 Conclusions

Based on the modeling, simulation, steady state analysis and experimental verification of the VSCF power conversion scheme with PMSG, the following conclusions are made:

i. A step-by-step procedure for modeling, simulation and analysis of the steady state performance of the VSCF power conversion scheme with PMSG has been formulated.

ii. Close correlation between the predicted and experimental results has been achieved in the power conversion scheme with the half-wave controlled converter.

iii. At part loads and at very low speeds, the efficiency of the power conversion scheme is very high.

iv. By substituting a PM rotor for wound rotor in the synchronous generator, two things have been achieved. They are:

1) A seperate dc supply for field excitation has been eliminated.

2) Need to control this field excitation is also removed.

v. The loss of external field current control has not affected the control and operation of the power conversion scheme.

vi. The proposed scheme is the simplest as it includes the control of only one variable, i.e. , triggering angle to the controlled converter to control the performance of the power conversion scheme.

5.3 Recommendations for future study

The following recommendations are made for future study:

i. Experimental verification of the power conversion scheme with the full-wave controlled converter.

ii. Transient analysis of the power conversion scheme.

iii. Comparison of VSCF power conversion schemes with wound rotor synchronous and induction generators.

Bibliography

1. P.W. Franklin, "Theory of the Three Phase Salient Pole Type Generator with Bridge Rectified Output," IEEE Trans vol. PAS-91, pp. 1960-1975, 1972.
2. P.W. Franklin, "A Theoretical Study of the Three Phase Salient Pole Type Generator with Simultaneous AC bridge Rectified DC output," IEEE Trans. vol. PAS-93, pp. 543-557,1973.
3. Z.M. Salameh and L.F. Kazda,"Analysis of Steady State Performance of the Double Output Induction Generator," IEEE Trans. on Energy Conversion vol. EC-1 NO 1, pp 26-32, March 1986.
4. Z.M. Salameh and L.F. Kazda,"Analysis of the Double Output Induction Generator Using Direct Three - Phase Model," IEEE Trans. on Energy Conversion Vol. EC-2 No.2, pp 175-187, June 1987.
5. R. Krishnan and A.j. Beutler, " Performance and Design of an Axial Field Permanent Magnet Synchronous Motor Servo Drive," IEEE IAS Annual Meeting, pp 634-640, 1985.
6. P. Pillay and R. Krishinan, " Modeling of Permanent Magnet Motor Drives," IEEE IAS Annual Meeting, pp 7-14, 1987.
7. P. Pillay and R. Krishinan, "Application Characteristics of Permanent Magnet Synchronous and Brussless DC Motor for Servo Drives," IEEE IAS Annual meeting, pp 380-389, 1987.

8. G.R. Slemon and A. Straughen, "Electric Machines," Addison-Wesley Pub. Co., 1981

9. B.M. Bird and K.G. King, "An Introduction to Power Electronics," Westinghouse Brake and Signal Co., 1983.

10. K. Heumann "Basic Principles of Power Electronics," Spring-Verlag, 1986.

11. David Finney, "The Power Thyristor and Its Applications," McGraw-Hill, 1980.

12. W. Kaplan, "Advanced Mathematics for Engineegs," Addison-Wesley Pub. Co., 1981.

Appendix-1.

1. PMSG parameters

R_s = 1.4 ohm. Stator resistance

L_d = 5.6 mH Stator d-axis inductance

L_q = 5.8 mH Stator q-axis inductance

p = 6 Number of poles

λ_m = 0.1546 V /(rad/sec) Mutual flux linkage

B = 0.00038818 Nm/(rad/sec) Damping constant

J = 0.00176 $Kg - m^2$ Moment of inertia

2. Legend for the SCR-control circuit

C Comparator

I Integrator

N And gate

555 Pulse Generator

A_f A-Phase firing circuit

B_f B-Phase firing circuit

C_f C-Phase firing circuit

V_{an} A-Phase voltage

V_{bn} B-Phase voltage

V_{cn} C-Phase voltage

Appendix-2.

1. List of symbols

I_g Generator line current

I_{g1} The fundamental component of the generator line current

I_{dc} DC link current

I_{ref} Reference current to control

I_m PMDC Input current

v_{ag}, v_{bg}, v_{cg} PMSG phase voltage

v_{at}, v_{bt}, v_{ct} Transformer phase voltage

v_t Transformer line to line voltage

V_{dc} DC voltage of the rectifier

V_i Inverted voltage of the controlled converter

V_m PMDC input voltage

V_c SCR control voltage

L_{dc} Link filter inductance

R_{dc} Link filter resistance

L_d, L_q Quadrature d,q axes inductance

α SCR triggering angle

μ Overlap angle due to the PMSG equivalent reactance

μ_t Overlap angle due to the transformer

ω_r PMSG angular speed

f_s Frequency of the ac supply

VITA

Mr. Geun-hie Rim was born in Jeon-Ju, Korea on october 7, 1955. He received the B.S. degree in Electrical Engineering from Seoul National University, Seoul, Korea in 1978. Since graduation he has worked for Korea Electrotechnology Research Institute, Chang-Won,Korea as a research engineer. During the course of this work he has been deputed for graduate study at Virginia Polytechnic Institute and State University by his employer.